nature communications

Article

https://doi.org/10.1038/s41467-025-67904-0

Neuropeptide SP protects against colitis and linked anxiety-like behavior through the putative roles of gut microbiota and metabolite inositol

Received: 5 September 2024

Accepted: 11 December 2025

Published online: 08 January 2026

Check for updates

Jing Lan[1], Jiaqi Wang[1], Sijuan Huang[1], Chenyu Li[1], Ziteng Deng[1], Zhihui Hao[1,2] & Yunfei Ma[1,2]

The gut-brain axis links gut inflammation to psychiatric symptoms in inflammatory bowel disease (IBD), but the underlying mechanisms remain unclear. We demonstrate that neuropeptide substance P (SP) alleviated intestinal injury and behavioral disorders induced by dextran sodium sulfate in mice. SP mitigated hippocampal neuroinflammation and inhibited microglial activation and astrocyte loss. Furthermore, SP improved gut microbiome dysregulation, and its protective effects depended on the putative roles of microbiota. Notably, through modulating microbiota, SP dampened the NF-κB pathway in microglia, and increased GABAergic/Ca^{2+} signaling within astrocytes. SP elevated the microbiota-derived metabolite inositol. Supplementing inositol mimicked SP's benefits and activated GABAergic signaling, while the inositol inhibitor reversed SP's neuroprotective impacts, highlighting inositol's indispensable role. Collectively, SP exerts beneficial effects via microbiota's putative roles and inositol, involving the suppression of microglial NF-κB pathway while enhancing astrocytic GABAergic/Ca^{2+} signaling. Our findings underscore SP's potential as a therapeutic intervention for these disorders in IBD.

Inflammatory bowel disease (IBD), which comprises ulcerative colitis and Crohn's disease, is a complex chronic and disabling illness that elicits gastrointestinal inflammation throughout life[1]. Recent research has found a strong association between the symptoms of intestinal lesions in IBD and psychiatric comorbidities[2]. Clinically, the occurrence of anxiety and depression is up to 30% and 25% in IBD patients[3]. Psychological disorders in IBD patients not only negatively affect the quality of life but also deteriorate the severity of the disease in suffering[4]. Regrettably, the mental health challenges associated with IBD tend to be given less attention than the intestinal manifestations of the disease. Despite the precise etiology behind the development of IBD and the related psychiatric comorbidities is complex, and not yet incompletely understood.

Accumulating evidence has suggested the composition of the gut microbiome not only impacts intestinal health but also controls brain physiological function through the gut-brain axis, which permits the bidirectional communication between the gut microbiome and the central nervous system (CNS), highlighting the significance of the microbiota-gut-brain (MGB) axis in neuroscience[5,6]. Imbalance of the gut microbiome may contribute to CNS impairments. Recent studies have illustrated that disrupting the intestinal microbiota of colitis mice can significantly impact the gut-brain axis, leading to neuroinflammation and brain pathology[7]. Transferring the microbiota of healthy individuals to the gastrointestinal tract of IBD patients alleviated gut inflamed symptoms and mental impairment[8]. Crucially, the metabolites produced by the gut microbiota have been reported

[1]State Key Laboratory of Veterinary Public Health and Safety, College of Veterinary Medicine, China Agricultural University, Beijing, PR China. [2]Innovation Centre of Chinese Veterinary Medicine, College of Veterinary Medicine, China Agricultural University, Beijing, PR China. e-mail: yunfeima@cau.edu.cn

to mediate host-microbiota interactions, showing the potential to regulate host physiology via the MGB axis[9]. However, little is known about how DSS-induced alterations in the gut microbiota and their derived metabolites impact centrally mediated systems implicated in mood, warranting further research.

The growing body of evidence indicates that gut microbiome imbalances can compromise intestinal barrier integrity, allowing the translocation of inflammatory molecules and noxious products generated by pathogenic bacteria from the gut lumen into the systemic circulation. These factors can then disseminate to the brain, thereby directly eliciting neuroinflammatory signaling cascades[10,11]. Neuroinflammation can alter the normal levels and interactions of key neurotransmitters in the brain, such as serotonin (5-HT), dopamine, and gamma-aminobutyric acid (GABA), which are important for regulating mood and behavior[12,13]. Undoubtedly, microglia, recognized as crucial players in neurodegenerative disorders, become persistently activated under inflammatory stimuli, leading to the production of neurotoxic mediators, including cytokines[14]. Therefore, a deeper understanding of the specific biomolecular pathways and signaling cascades that mediate the influence of the gut microbiome on neuroinflammation would be essential to advance the field of research on mood disturbances. Additionally, as the most abundant cells within the brain, astrocytes were activated and transited into reactive astrocytes post-CNS injury[15]. Astrocytes are implicated in the remodeling of the CNS through their dual roles. For another, reactive astrocytes secrete a diverse array of pro-inflammatory cytokines, and chemokines[16]. For one thing, they release neurotrophic factors, maintain synaptic neurotransmitter levels, and transmit information through gap junctions and calcium waves[17–19]. Interestingly, the latest research has suggested that a specific subgroup of astrocytes, which are regulated by the gut microbiome, exhibit a protective anti-inflammatory function within the brain. It cannot be denied that the current body of work on anxiety has so far centered on hippocampal neurons and neural circuits linked to the disorder. In contrast, the action mechanism of hippocampal astrocytes in anxiety has not been sufficiently addressed. Regardless, these findings provide evidence that gut microbiota has been recognized as a pivotal regulator between gut and brain signal transduction. Targeting the modulation of the intestinal microbiota and of the produced metabolites seems to be a very potential approach for the treatment or prevention of dysbiosis-driven disorders.

Over the past few years, various researchers have reported that neurotransmitters, known as a crucial mediator in the crosstalk between the gut and brain, possess the ability to affect the intestinal microbial community[20]. Neuropeptides such as substance P (SP) are generated at all levels of the MGB axis, and they contribute substantially to the bidirectional signaling processes occurring between the gut and brain[21]. In principle, the gut microbiota would be expected to exhibit a response to neuropeptides, if it were to possess the corresponding receptor[21]. Nonetheless, there remains a lack of direct evidence supporting the involvement of SP in the communication between microbial communities within the gut and the CNS. SP has been implicated in the modulation of various psychiatric disorders. On one hand, several studies indicate SP's involvement in the pathophysiological processes. For example, Schwarz et al. reported that SP concentration is elevated under stress, and that pharmacological antagonism or genetic depletion of NK-1 receptors results in an anxiolytic response, suggesting SP as a potential therapeutic target for treating stress and anxiety-related disorders[22]. On the other hand, the neuroprotective effects of SP have garnered significant attention. SP has been shown to promote memory, reinforce learning, and exhibit anxiolytic-like effects when administered systemically or directly into the nucleus basalis of the ventral pallidum[23]. Furthermore, SP may counteract the neurotoxicity of beta-amyloid protein, a key factor in the neuropathology of Alzheimer's disease, and could also have beneficial effects in the context of Parkinson's disease and its related models[24]. Moreover, Ahn et al. demonstrated that SP mitigates functional impairments resulting from a partial 6-hydroxydopamine lesion of the nigrostriatal system and provides neuroprotection in ischemic stroke by regulating M2 microglia polarization[25]. Our previous work has demonstrated the ability of SP to improve DSS-induced acute colitis, showing that SP counteracted the inflammatory response and ferroptosis triggered by DSS exposure[26]. It also remains to be investigated whether and how SP alters the gut microbial impacts on the intestinal barrier dysfunction and CNS in anxiety-like symptoms in IBD.

In this study, we investigated the protective effects of SP against dextran sodium sulfate (DSS)-induced pathological features of colitis, as well as hippocampal neuroinflammation and behavioral disorders in mice. We explored the ability of SP to improve microbial dysbiosis and further verified the putative role of gut microbiota and microbiota-derived metabolite inositol in SP's beneficial impacts on intestinal impairment and anxiety-like behavior through fecal microbiota transplantation (FMT), antibiotic treatment, and inositol supplementation. Importantly, we demonstrated that the neuroprotective activity of SP was achieved through the suppression of the NF-κB pathway within microglia and the enhancement of GABAergic neurotransmission and downstream Ca^{2+} signaling within astrocytes in the hippocampus.

Results

SP ameliorates colitis symptoms and anxiety-like behaviors in DSS-induced mice

In this study, we used DSS treatment to successfully induce colitis mouse model which is a widely used chemically induced model resembling human ulcerative colitis[27]. As shown in Fig. 1a, mice were given DSS through their drinking water and were administrated intravenously with SP. In order to assess the role of SP in the pathogenesis of colitis, the weight, rectal bleeding, and stool consistency of the mice were monitored. Supplementation of SP remarkably mitigated the gross symptoms of colitis (Fig. 1b–d and Supplementary Fig. 2a). As shown in Fig. 1e, the colon tissue of normal mice was observed without inflammatory cell infiltration or mucosal erosion. In contrast, mice in the DSS group displayed intestinal mucosal and submucosal edema, severe inflammatory cell infiltration, crypt loss, and epithelial injury. The histological scores of the DSS-treated mice were significantly higher than those of the normal mice. Administration with SP showed protective effects on the colon, with intact crypts and mucosal epithelial cells, and no significant edema or inflammatory cell infiltration observed in the submucosa. Consistently, histological scores were significantly decreased by SP administration compared to the DSS-treated group. Crypt depth was markedly declined in the DSS group, but this was alleviated following SP administration (Supplementary Fig. 2b). As illustrated in Fig. 1f, transmission electron microscopy (TEM) analysis revealed intact intestinal epithelium in the CON group, with neatly arranged microvilli. The DSS group exhibited irregularities in the colonic epithelium, characterized by widened intercellular spaces as well as shortened and curated microvilli. Conversely, SP treatment effectively mitigated these changes. Prior research has indicated that mucin and goblet cells serve as the basic lines of defense to safeguard the gut[28]. We explored the role of SP on goblet cells in the colon during colitis. Acidic mucous substances were stained lake blue using Alcian Blue (AB), while neutral mucous substances were stained purple blue with Periodic Acid-Schiff (PAS)[29]. As illustrated in Fig. 1g, AB-PAS staining revealed that positively stained goblet cells in the colonic mucosa were densely distributed on both sides of the crypts, exhibiting a regular and full shape in the normal group of mice. In contrast, the DSS group exhibited only a few crypts remaining in the lamina, leading to a notable decrease in the number of positively stained goblet cells that contain mucus. However, following treatment with SP, the loss of goblet cells was remarkably alleviated. Mucin 2 (MUC-2), produced by goblet cells, is a major component of the colonic mucus barrier[30]. Immunofluorescent staining revealed that

https://doi.org/10.1038/s41467-025-67904-0

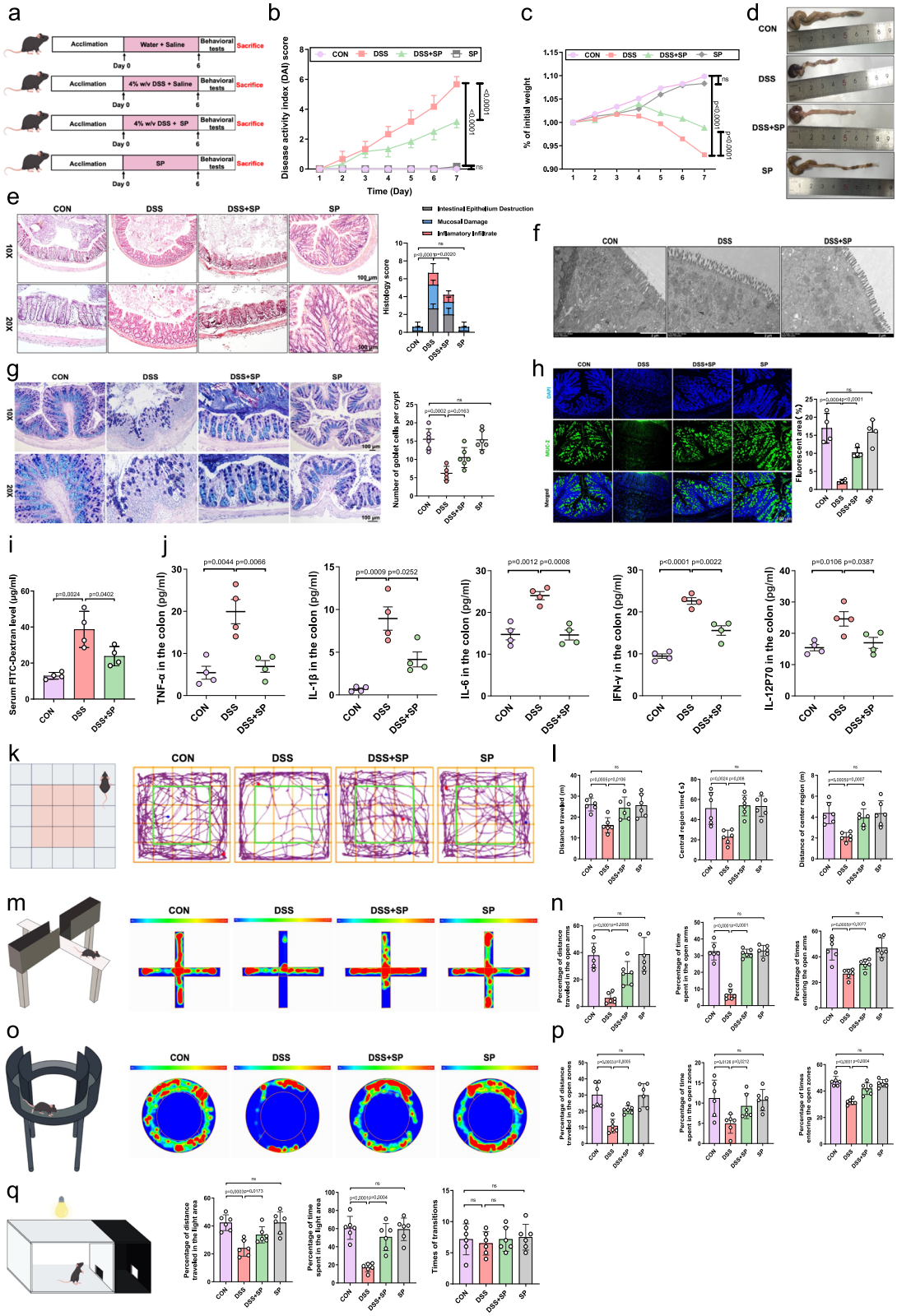

the secretion of MUC-2 in DSS-induced colitis was significantly decreased compared to the CON group. Conversely, an increase in MUC-2 expression was observed following SP administration (Fig. 1h). Increased intestinal permeability allows foreign substances to enter and compromises the integrity of the barrier function[31]. We next assessed intestinal permeability by measuring serum levels of FITC-dextran. The serum levels of FITC-dextran were markedly elevated in DSS-induced mice compared to those in the CON group; however, this elevation was mitigated by SP administration (Fig. 1i). The results indicate that SP effectively repaired the impairment of the intestinal barrier and decreased the permeability of the intestinal epithelium. Previous study has shown that excessive pro-inflammatory factors are associated with the destruction of the intestinal epithelium[32]. We further measured the levels of inflammatory cytokines in the colon tissues

Fig. 1 | SP ameliorates colitis symptoms and anxiety-like behaviors in DSS-induced mice. a Study design for study 1 (Some schematic elements were created by Figdraw.com), and a detailed description is provided in the Methods section. **b** Daily DAI throughout the entire duration of the study. n = 8 mice/group. **c** Percentage body weight change. n = 8 mice/group. **d** Colon lengths image. **e** Representative images of hematoxylin and eosin-stained colonic sections, and histology scores. Scale bar = 100 μm. n = 6 mice/group. **f** Microvilli in the ultrastructure of the colon observed by TEM. Scale bar = 2 μm. n = 5 independent experiments. **g** Representative images of alcian blue-stained colonic sections, and the number of goblet cells per crypt. n = 6 mice/group (CON, DSS + SP, SP) and 5 mice/group (DSS). **h** Immunofluorescence staining for MUC2 (green) with DAPI (blue) in colonic tissues and statistical analysis, Scale bar =100 μm. n = 4 mice/group. **i** The concentration of FITC-Dextran in serum. n = 4 mice/group. **j** The levels of inflammatory cytokines in colon tissues. n = 4 mice/group. **k** Diagram of the open-field test (Created by Figdraw.com) and representative track image. **l** Total distance traveled, time spent and distance traveled in the central region. n = 6 mice/group. **m** Diagram of the elevated plus maze (Some schematic elements were created by Figdraw.com) and representative track image. **n** Percentage of distance traveled in the open arms, percentage of time spent in the open arms, and percentage of times entering the open arms. n = 6 mice/group. **o** Diagram of the elevated zero maze (Some schematic elements were created by Figdraw.com) and representative track image. **p** Statistical analysis (percentage of distance traveled in the open zones, percentage of time spent in the open zones, and percentage of times entering the open zones). n = 6 mice/group. **q** Diagram of the light-dark box (Created by Figdraw.com) with statistical analysis (percentage of distance traveled in the light area, percentage of time spent in the light area, and transitions between the two boxes). n = 6 mice/group. Data were presented as means ± SD. For DAI score and body weight change, two-way repeated-measures ANOVA was performed and the rest of the statistics was analyzed using one-way ANOVA followed by Tukey's multiple comparisons test. $^{*}P \le 0.05$, $^{**}P \le 0.01$, $^{***}P \le 0.001$. Source data are provided as a Source Data file.

using Luminex multiplex assays (Fig. 1j). The amounts of TNF-α, IL-1β, IL-6, IFN-γ and IL-12P70 were dramatically higher in the DSS group than in the CON group. Of particular note, after SP administration, levels of TNF-α, IL-1β, IL-6, IFN-γ and IL-12P70 were reduced. Intriguingly, no obvious clinical symptoms or histopathologic changes were observed in the SP alone-treated group compared to the CON group. These data suggest that SP could preserve the integrity of the intestinal barrier and alleviate colonic inflammation.

There is a growing body of evidence suggesting that anxiety-like behaviors are commonly observed in patients with IBD, but the impact of SP on IBD-linked behavior abnormalities has not been substantiated. In the present study, we employed the open-field test (OFT), elevated plus-maze (EPM), elevated zero maze (EZM) and light-dark box (LDB) to assess the effects of SP on anxiety-like behaviors in DSS-induced mice. In the OFT test, the total distance in the entire area, as well as the time spent and distance moved in central region in the DSS group was dramatically less than that in the CON group, demonstrating that DSS remarkably reduced the autonomous activity and exploration desire of mice. However, SP significantly reversed this phenomenon (Fig. 1k, l). Moreover, the potential anxiolytic-like activity of SP, as assessed by the EPM in mice, is presented in Fig. 1m, n and Supplementary Fig. 3a. The results demonstrated that the DSS group exhibited decreased percentage of distance traveled and time spent in the open arms, along with fewer percentage of open-arm entries and reduced total distance traveled, compared to the CON group. In contrast, SP treatment effectively reversed DSS-induced behavioral alterations. As a modification of the EPM, EZM is used to assess anxiety-like behaviors[33]. We examined the anxiolytic effects of SP by the EZM test. As shown in Fig. 1o, p and Supplementary Fig. 3b, the percentage of distance traveled and time spent in the open zones, the percentage of times entering the open zones and total distance traveled in the DSS group were significantly lower than those in the CON group. However, the DSS + SP group showed significantly greater percentage of distance traveled and time spent in the open zones, percentage of times entering the open zones and total distance traveled compared to the model group. In the LDB test, compared to the CON group, mice exposed to DSS exhibited lower percentage of distance traveled and percentage of time spent in the light box, indicating that DSS exposure decreased the exploration desire of the mice, along with fewer total distance traveled. Conversely, SP treatment increased the percentage of distance traveled in the light box, percentage of time spent in the light box and total distance traveled (Fig. 1q and Supplementary Fig. 3c). Additionally, the mice could freely move between the light and dark boxes, with the number of passages through the door shown in Fig. 1q. However, no differences in the transition frequencies were observed among the four groups. Notably, no statistically significant differences were observed between the CON group and the SP alone-treated group across all behavioral analyses. Collectively, these data suggest that SP protects against anxiety-like behaviors of mice with colitis.

Considering that potential malaise-induced by the inflammation might affect the anxiety behavioural readout, we assessed the anxiety-like behavior when colonic inflammation was eliminated. As shown in Supplementary Fig. 4a-c, following DSS withdrawal (day 15), the DAI and colonic tissue structure in the DSS and DSS + SP groups were recovered to the levels of the normal group. To further, we examined the anxiolytic effects of SP using the OFT and EPM test. In the OFT test, less time was spent and a shorter distance was traveled in the central area in DSS-treated mice compared with the CON group. In contrast, SP remarkably improved these behavioral changes (Supplementary Fig. 5a-c). In the EPM test, the percentage of open-arm entries, as well as the percentage of time spent and distance traveled in the open arms were significantly decreased in the DSS group than the CON group. However, SP profoundly reversed these alterations (Supplementary Fig. 5e-h). Notably, no significant differences in the total distance traveled were observed among the three groups in the OFT and EPM test, indicating locomotor activity was recovered (Supplementary Fig. 5d, i). These results indicate that anxiety-like behavior associated with colitis is persistent, even after the potential discomfort induced by intestinal inflammation has resolved; meanwhile, SP exerts anxiolytic effects.

SP mitigates hippocampal damage and neuroinflammation in DSS-induced mice

Hippocampal impairment can affect the function of the emotional regulation center, which may lead to psychiatric disorders, such as depression and anxiety[34,35]. Therefore, H&E staining has been utilized to evaluate morphological changes in the hippocampus of each group. As shown in Fig. 2a, b, significant pathological changes, such as neuronal loss, nuclear condensation, and neuronal shrinkage, were observed in the DSS group. However, cell bodies were clearly visible, and appeared continuous and uniform, without obvious disruptions in the DSS + SP group. Notably, no apparent pathological changes were observed between the SP treatment alone and the CON group. Nissl staining was performed to analyze the potential effects of SP on the neuronal cell distribution. The results showed that the DSS group exhibited a large loss of Nissl bodies and disorganized and loosely arranged cells within the DG region of the hippocampus. In contrast with the DSS group, SP markedly attenuated the neuronal damage caused by DSS, helping to preserve neuronal morphological structure and the number of Nissl bodies. The neuronal density and distribution within the CA1 and CA3 regions did not exhibit any obvious changes among the four groups (Fig. 2c, d). The neuroinflammatory response has been demonstrated to aggravate hippocampal impairment and disrupt the important balance of neurotransmitters, thereby affecting emotional regulation and causing anxiety-like disorders[13,36]. Here, to explore the role of SP in mitigating neuroinflammation,

https://doi.org/10.1038/s41467-025-67904-0

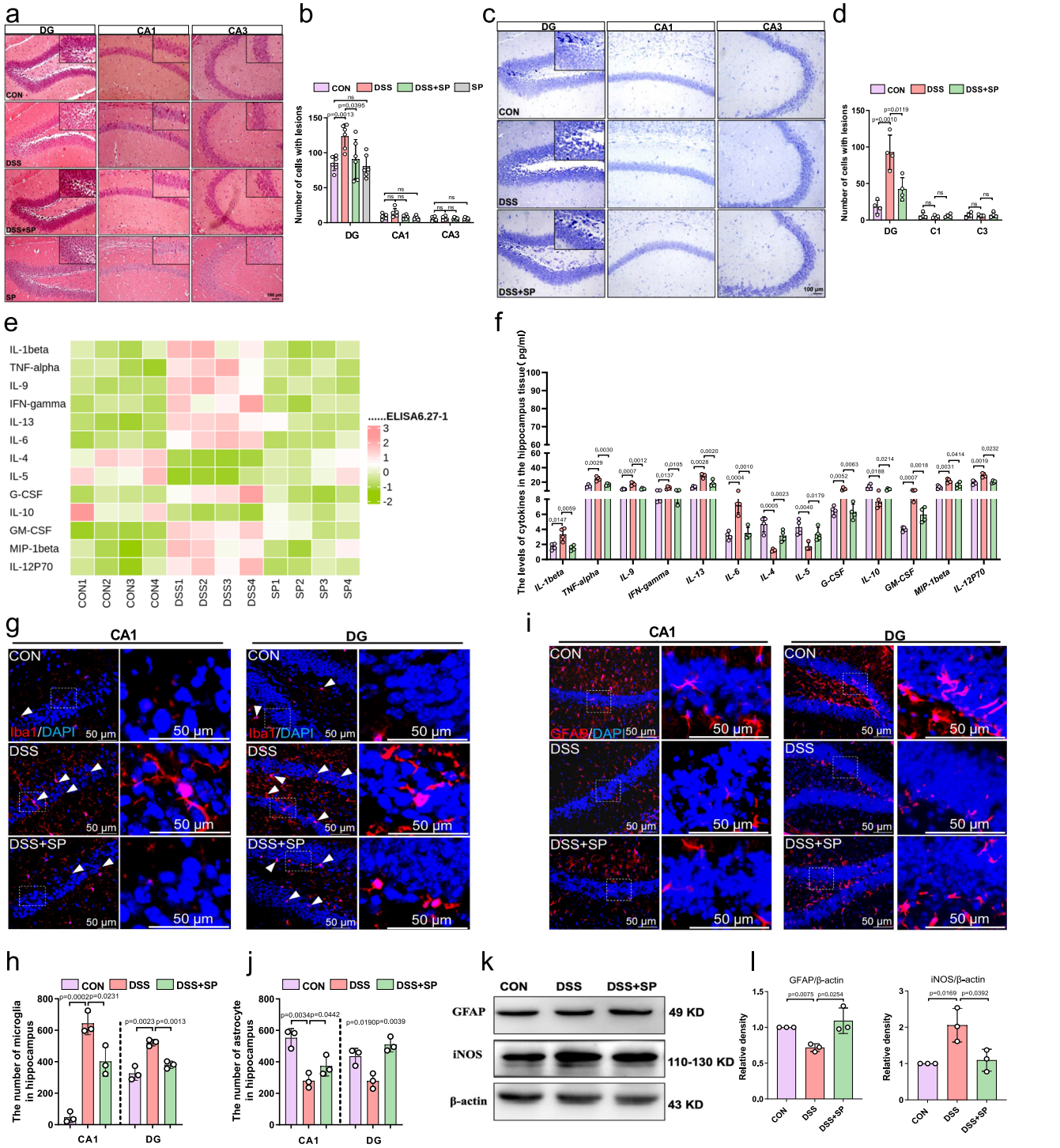

Fig. 2 | SP mitigates hippocampal damage and neuroinflammation in DSS-induced mice. a, **b** Representative image of H&E staining in the hippocampus and quantification of cells with lesions. n = 6 mice/group. **c**, **d** Representative images of Nissl staining and quantification of hippocampal neurons with lesions. n = 4 mice/group. **e, f** Heatmaps and concentrations of representative pro-inflammatory cytokines, IL-1β, TNF-α, IL-9, IFN-γ, IL-13, IL-6 IL-4, IL-5, G-CSF, IL-10, GM-CSF, IL-10, GM-CSF, MIP-1β and IL-12P70 in the hippocampus. n = 4 mice/group. **g**, **h** Immunofluorescence images of DAPI (blue) and Iba-1 (red) in the DG region of the hippocampus, and quantitative analysis of the number of Iba-1-positive microglia. Scale bar = 50 μm. n = 3 mice/group. **i**, **j** Immunofluorescence images of GFAP (red) and DAPI (blue) in the DG region of the hippocampus, quantitative analysis of the number of GFAP-positive astrocytes. Scale bar = 50 μm. n = 3 mice/group. **k** Western blot analysis of GFAP and iNOS protein expressions in the hippocampus. **l** Quantification of normalized values of GFAP and iNOS levels with β-actin. n = 3 independent experiments. Data were presented as means ± SD. Statistical significance was determined using one-way ANOVA followed by Tukey's multiple comparisons test. $^{*}P \le 0.05$, $^{**}P \le 0.01$, $^{***}P \le 0.001$. Source data are provided as a Source Data file.

we investigated the concentrations of inflammatory mediators in the hippocampal tissue (Fig. 2e, f). The results showed that SP significantly decreased the levels of IL-1beta, TNF-alpha, IL-9, IFN-gamma, IL-13, IL-6, G-CSF, GM-CSF, MIP-1bata, and IL-12P70, but elevated the levels of IL-4, IL-5, and IL-10 in the hippocampus of DSS-treated mice. These results suggest that SP mitigates DSS-induced hippocampal neuroinflammation by modulating the balance between proinflammatory cytokines and anti-inflammatory factors.

Previous studies have demonstrated the activation of microglia in response to neuroinflammation[37]. In addition, astrocytes also have the capacity to exhibit anti-inflammatory and neuroprotective activities in the context of neuroinflammation like in Parkinson's disease or multiple sclerosis[38]. To investigate how SP affects microglia/astrocytes, we counted the two cell types in the hippocampus of each group. As illustrated in Fig. 2g, h, immunofluorescence analysis was performed for DG and CA1 regions, and the results showed the number of Iba-1-positive microglia cells was elevated in the DSS group compared to the CON group; however, the SP group exhibited a significant down-regulation in the Iba-1-positive cells. By contrast, an increase in the astrocyte marker GFAP-positive cells was observed in the SP group compared to the DSS group (Fig. 2i, j). The M1 phenotype of microglia is closely associated with the promotion of neuroinflammation. Activated M1 microglia secrete pro-inflammatory mediators to exacerbate neuronal damage and disrupt the homeostatic function of the CNS[39]. To elucidate the characteristic phenotype of activated microglia, the expression of M1-associated marker iNOS was analyzed by western blot. As shown in Fig. 2k, l, the protein level of iNOS was markedly increased in DSS-treated mice compared with the mice from the CON group, whereas supplementation with SP reversed this alteration. Concurrently, the western blot data showed results consistent with the immunofluorescence analysis, revealing increased protein expression of GFAP after SP treatment (Fig. 2k, l). It can be reasonably inferred that SP ameliorated the anxiety-like behavior in colitis mice by dampening pathological lesions and neuroinflammation in the hippocampus, which might be related to suppressing the polarization of microglia towards the M1 phenotype and preventing astrocytes loss.

SP ameliorates gut microbial dysbiosis and alters microbiome functions in DSS-induced mice

To evaluate whether SP could cross the blood-brain barrier and directly affect the brain, we assessed the expression of SP in the hippocampus among different groups using ELISA. We found no significant differences in the concentration of SP among the CON, DSS, and DSS + SP groups (Supplementary Fig. 6a). Additionally, SP is produced by enzymatic cleavage of the precursor protein (perprotachykinin-A). RT-qPCR analysis revealed that, following SP administration, the mRNA expression of *TAC1* encoding preprotachykinin-A in the hippocampus of the DSS + SP group did not differ significantly from that in the DSS group (Supplementary Fig. 6b). These results suggest that administration of SP could not effectively cross the blood-brain barrier to exert its effects on the brain.

Emerging research has established a strong link between alterations in the gut microbiome and anxiety-related conditions. To investigate whether SP could mitigate the microbiota imbalances induced by DSS exposure, the composition of gut microbiota was analyzed using 16S rRNA gene sequencing. We evaluated the alteration in α-diversity using the Shannon index. Compared with DSS induction, SP did not appear to have a significant impact on the richness and diversity of intestinal flora (Fig. 3a). To fully assess the β-diversity of microbial communities, the overall structure of gut microbiota was defined using a principal 1 analysis (PCoA) based on the binary Jaccard distance (Fig. 3b). Significant differences in β-diversity were observed across the CON, DSS, and DSS + SP groups (PERMANOVA, $p = 0.001$), indicating that the bacterial community structures were significantly different. At the phylum level, compared with the CON group, the DSS group showed enrichments in *Bacteroidetes*, and *Proteobacteria*, whereas compared with the DSS group, the DSS + SP group exhibited a higher relative abundance of *Firmicutes* (Fig. 3c). At the family level, the relative abundance of *Bacteroidaceae* and *Enterobacteriaceae* was elevated in the DSS group compared to that in the CON group, while the relative abundance of *Lachnospiraceae* and *Muribaculaceae* was significantly increased in the DSS + SP group, compared with that in the DSS (Fig. 3d). At the genus level, the relative abundance of *Bacteroides* and *Alistipes* was reduced, and that of *unclassified_Lachnospiraceae*, *unclassified_Muribaculaceae* and *Lachnospiraceae_NK4A136_group* was up-regulated in the DSS + SP group, compared with those in the DSS group (Fig. 3e). The random forest analysis predicted that g_*Unclassified_Christensenellaceae* and g_*Parasutterella* could be prominent bacterial classification, which had a significant impact on the differences between groups (Fig. 3f). One-way analysis of variance (ANOVA) was performed to compare the relative abundance of dominant species among the three groups. At a phylum level, a significantly higher abundance of p_*Firmicutes* was observed in SP-treated mice compared to DSS-treated mice. DSS exposure provoked a substantial escalation in the abundance of p_*Bacteroides*, which was also dramatically reversed by SP (Fig. 3g). Meanwhile, at the genus level, g_*Bacteroides* and g_*Escherichia_Shigella* were notably reduced in abundance in the SP group compared to the DSS group, whereas g_*unclassi®ed_Muribaculaceae*, g_*Prevotellaceae*_UCG_001, g_*Candidatus_Arthromitusm* as well as g_*unclassified_Lachnospiraceae* were remarkably more abundant in the SP group (Fig. 3h, i). Phylogenetic Investigation of Communities by Reconstruction of Unobserved States (PICRUSt2) analysis was used to predict intestinal microbial metabolic function. Compared with the CON group, several functional modules in the DSS group (e.g., Pentose phosphate pathway, Biofilm formation-Vibrio cholerae, Glycerolipid metabolism, Quorum sensing, Photosynthesis) were found to be suppressed (Fig. 3j). In contrast, the DSS + SP group exhibited increased activity in functional modules, such as Nucleotide excision repair, Inositol phosphate metabolism, Methane metabolism, Bile secretion, NOD-like receptor signaling pathway, Epithelial cell signaling in Helicobacter pylori infection and Mineral absorption) compared to the DSS group (Fig. 3k). Overall, these data suggest that the administration of SP protected against DSS-induced gut microbiota dysbiosis in mice.

Additionally, we investigated the regulatory effects of SP on the composition of gut microbiota using 16S rRNA sequencing analysis of colonic content in non-colitis mice. Notably, the α-diversity analysis, as assessed by the Shannon index, revealed no significant differences in bacterial richness and diversity between the two groups (Supplementary Fig. 7a). The overall structure of the gut microbiota, investigated using binary Jaccard-based PCoA, indicated that the SP group displayed a shift in the clustering of bacterial composition, which was distinct from the CON group, suggesting that SP treatment induced changes in the gut microbiota composition (Supplementary Fig. 7b). We then analyzed the gut bacterial composition at the genus level. Results revealed that SP significantly reduced the relative abundance of *Limosilactobacillus* and *Bacteroides* relative to control mice. Conversely, the abundance of *unclassified_Muribaculaceae*, *Lachnospiraceae_NK4A136_group*, and *unclassified_Lachnospiraceae* was significantly increased in SP-treated mice compared to those in control mice (Supplementary Fig. 7c). The differences in the relative abundance of gut microbiota at the genus level between the CON group and the SP group were analyzed using ANOVA (Supplementary Fig. 7d).

SP protects against intestinal damage and anxiety-like disorders induced by DSS through modulating the gut microbiota

Given our evidence that SP effectively regulates gut microbiota to alleviate colitis, we probed further into the putative role of gut microbiota in mitigating colitis and anxiety-like behaviors following SP treatment. To this end, antibiotic treatment on mice for 14 days was carried out to eliminate the gut microbiota, as depicted in Fig. 4a. At the end of the ABX treatment (on day 14), the addition of antibiotics dramatically depleted the microbiota under aerobic conditions (Fig. 4b, c). Following DSS treatment (on day 21), the microbiota remained significantly reduced compared to the normal group, although a slight increase was observed. Additionally, fecal DNA analysis revealed that the fecal DNA from mice treated with antibiotics (on day 14) and continuously treated with DSS for 6 days (on day 21) was lower than that of the normal mice

https://doi.org/10.1038/s41467-025-67904-0

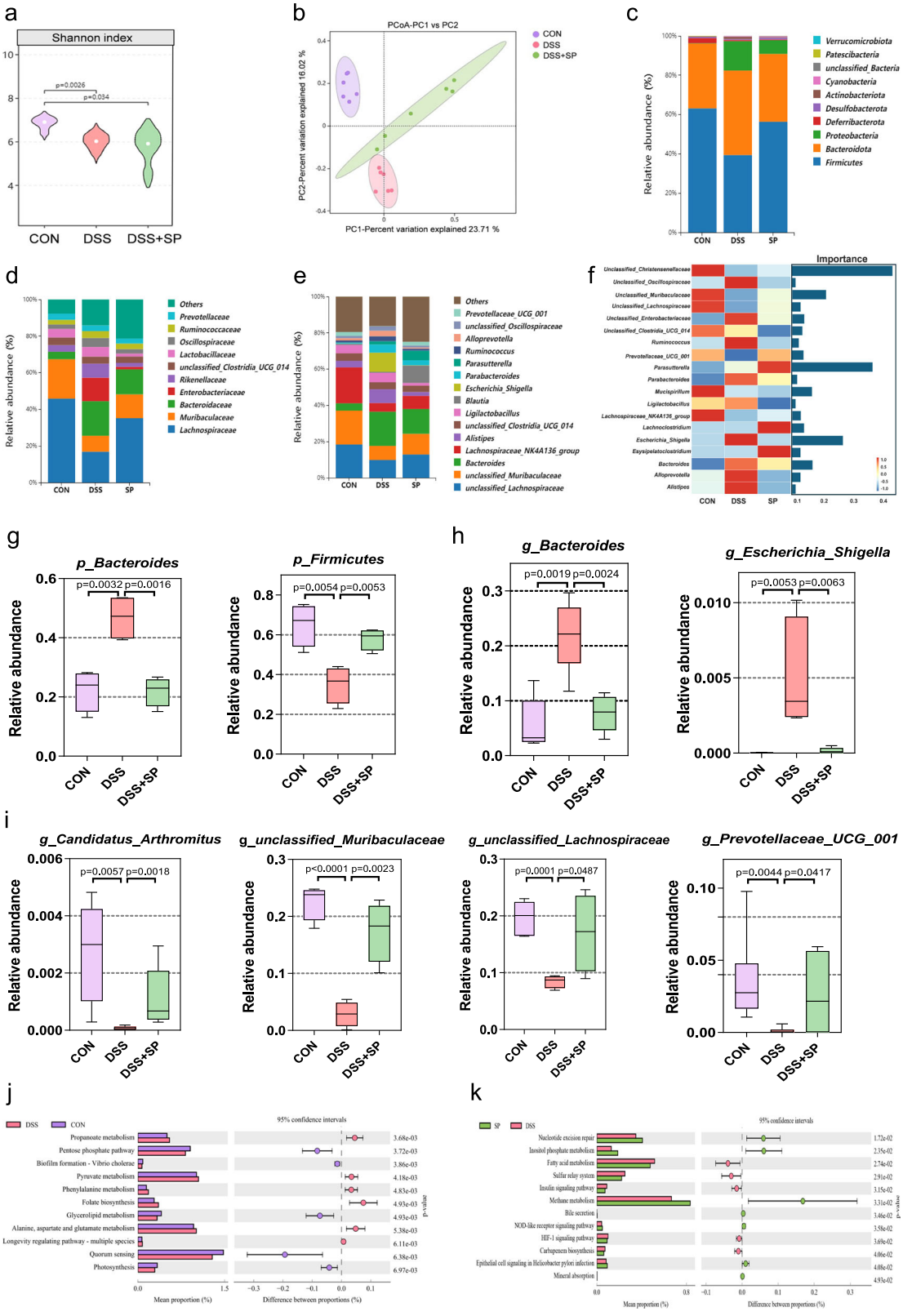

(Supplementary Fig. 8a). Antibiotic-induced perturbation of the microbiota can disrupt intestinal homeostasis and compromise the integrity of intestinal defenses[40]. As expected, the significant enlargement of the cecum was consistent with the typical characteristics observed in pseudo-germ-free (PGF) mice compared to those in untreated mice (Fig. 4f). These results indicate that the administration of the antibiotic cocktail disrupted microbiota composition and effectively depleted gut microbiota by days 14 and 21, suggesting that a PGF mouse model was successfully established.

Subsequent analysis indicated that antibiotic intervention had no significant effect on the body weight of healthy mice (Supplementary Fig. 8b). Strikingly, the beneficial effects of SP on clinical symptoms, such as DAI (Fig. 4d), body weight (Fig. 4e), colonic length (Fig. 4f and Supplementary Fig. 9a), spleen/body weight ratio (Fig. 4g and

Fig. 3 | SP ameliorates gut microbial dysbiosis and alters microbiome functions in DSS-induced mice. a α-diversity represented by the Shannon index, with two-sided one-way ANOVA. **b** Principal coordinates analysis (PCoA) of gut microbial based on the binary Jaccard distance. PERMANOVA: $R^2 = 0.331$, two-sided *P* value = 0.001. PERMANOVA: permutational multivariate analysis of variance. **c** Taxonomic distributions of gut bacterial composition at the phylum level. **d** Taxonomic distributions of gut bacterial composition at the family level. **e** Taxonomic distributions of gut bacterial composition at the genus level. **f** Important bacteria based on the random forest analysis. **g–i** ANOVA shows the relative abundance of the dominant gut microbiota in each group, at the phylum level and genus level, respectively. n = 6 mice/group. The whiskers indicate the minimum and maximum values observed within the range of Q1 − 1.5 × IQR to Q3 + 1.5 × IQR. The box reveals the interquartile range (IQR) between the 25th (Q1) and 75th (Q3) percentiles, and the line inside the box represents the median (50th percentile). **j, k** Differential analysis of PICRUSt2-predicted gut microbiome function based on the KEGG database. *P*-values was determined using two-tailed Student's *t* test. n = 6 mice/group. Error bars represent the proportion of differences in the abundance of functional microbiota within a 95% confidence interval. n = 6 for 16S rRNA gene sequencing. Source data are provided as a Source Data file.

Supplementary Fig. 9b), and intestinal structural integrity (Fig. 4h-k and Supplementary Fig. 9c), were notably weakened in the absence of the intestinal microbiome in mice. Consistently, anxiety-like behaviors improved by SP treatment was completely reversed after gut microbiota depletion (Fig. 4l-m). These results indicate that gut microbiota might exert effects in SP's protection against colitis and anxiety-like behavior.

To further confirm the putative role of gut microbiota in SP's protective effects, we transplanted the feces of CON, DSS, and DSS + SP donor mice into recipient mice for one week (Prior to FMT, all recipient mice were pretreated with antibiotics for 14 days). As shown in Fig. 5a, the FMT-DSS + SP group, which received feces from the DSS + SP group showed less body weight loss (Fig. 5b), lower DAI (Fig. 5c), relieved the colon shortening (Fig. 5d, e) and decreased spleen/body weight ratio (Supplementary Fig. 10a, b) when compared to the FMT-DSS group, which received feces from the DSS group. As illustrated in Fig. 5f, the mice subjected to FMT-DSS induction exhibited pronounced histological damage, featuring epithelial impairment, crypt loss, and inflammatory cell infiltration, but these pathological changes were notably ameliorated following FMT-DSS + SP treatment, as evidenced by lower histological scores and increased crypt depth (Supplementary Fig. 10c). AB-PAS staining revealed that in the process of colitis, the reductions in acidic and neutral mucin abundances, as well as the quantity of goblet cells, were largely restored to normal levels through FMT from SP-treated donor mice (Fig. 5g, h). To assess the effects of FMT-DSS + SP treatment on cytokines, we measured the concentrations of inflammatory factors in the colon using ELISA. Elevated levels of TNF-α and IL-6 were observed in the colon of the FMT-DSS group; however, these levels were attenuated following FMT-DSS + SP treatment (Fig. 5i). Moreover, myeloperoxidase (MPO), an enzyme found in neutrophils, serves as a common index for inflammation, with increased MPO activity indicating greater neutrophil infiltration in the colon[41]. FMT-DSS treatment resulted in increased MPO activity compared to FMT-CON mice, while FMT-DSS + SP treatment significantly reduced MPO activity (Fig. 5i).

We investigated the influence of FMT from DSS + SP-treated mice on the behavioral characteristics of mice with colitis. To begin, an open field test was performed to assess their anxiety-like behavior. Shortened distance traveled in the center area, less time spent in the center area and shortened total distance moved were shown in mice with colitis treated by FMT-DSS compared with the FMT-CON group. However, FMT-DSS + SP treatment profoundly improved these behavioral changes in the FMT-DSS group (Fig. 5j, k). Also, H&E staining was conducted to validate the histopathological alterations observed in the hippocampus. As shown in Fig. 5l, cell degeneration and damaged nuclei or nuclear shrinkage were augmented in the FMT-DSS mice compared to the FMT-CON group in DG and CA3 regions. All of these observed effects were alleviated through FMT-DSS + SP treatment. In Fig. 5m, the mRNA levels of inflammatory cytokines such as *TNF-α* and *IL-1β* in the hippocampus exhibited an obvious upward trend in the DSS group, and the mRNA expression of *IL-4* was down-regulated, but FMT-DSS + SP treatment was able to impede the alterations induced by FMT-DSS. Besides, no significant difference was observed in the mRNA expression of *IL-6* between the FMT-DSS and FMT-DSS + SP groups. Similarly, western blot analysis showed that the protein levels of iNOS and CD80 were significantly down-regulated in the hippocampus of the FMT-DSS + SP group when compared to the FMT-DSS group, however, FMT-DSS + SP treatment significantly suppressed the FMT-DSS-induced decrease in the protein expression of CD206 (Fig. 5n and Supplementary Fig. 11a-c). Additionally, FMT from DSS + SP-treated mice had a significant upregulation in the protein expressions of GFAP compared with FMT from DSS-treated mice, implying FMT-DSS + SP treatment could inhibit the decline of astrocytes induced by FMT-DSS treatment (Fig. 5n and Supplementary Fig. 11d). To clarify the characteristic phenotype of the activated microglia in the hippocampus, the co-localization of the iNOS (M1-associated marker) or CD206 (M2-associated marker) with Iba-1 was analyzed using double-labeled immunofluorescence staining, respectively. The data showed that after FMT-DSS treatment, the number of iNOS-immunopositive ($iNOS^+$) cells increased in the hippocampus, including the CA1 and DG regions. However, the numbers were significantly lower in the FMT-DSS + SP group than in the FMT-DSS group (Fig. 5o and Supplementary Fig. 11e). As well, we observed CD206-immunopositive ($CD206^+$) microglia were few after FMT-DSS treatment, whereas compared with the FMT-DSS group, the FMT-DSS + SP group showed a dramatic increase in the number of $CD206^+$ microglia (Fig. 5p and Supplementary Fig. 11f).

The donor microbiota was sourced from the CON, DSS, and DSS + SP groups, of which the composition of the gut microbiota was shown in Fig. 3. To investigate the microbiota reconstruction in the recipient groups, we analyzed the gut microbiota in the colonic content of FMT-CON, FMT-DSS, and FMT-DSS + SP mice using 16S rRNA gene sequencing analysis. Firstly, the Shannon index, indicative of intestinal flora richness, showed an increase in the diversity of intestinal microbiota in the FMT-DSS + SP group, compared to the FMT-DSS group, although no significant differences were observed between groups (Supplementary Fig. 12). PCoA using binary Jaccard distances demonstrated that the gut microbiota from these three groups was distinctly separated, indicating differences in microbial composition (Fig. 5q). As seen in Fig. 5r, FMT-DSS + SP treatment increased the abundance of p_*Firmicutes* and p_*Bacteroidetes* while decreasing the abundance of p_*Proteobacteria* in comparison with the FMT-DSS group. Furthermore, FMT-DSS + SP treatment resulted in an increase in the abundances of g_*unclassified_Muribaculaceae* and g_*unclassified_Lachnospiraceae*, while the relative abundances of g_*Bacteroides* and g_*Ligilactobacillus* were reduced compared to those in the FMT-DSS group (Fig. 5s). ANOVA was conducted at the genus level to identify the species for relative abundance box plot analysis, allowing for comparison of the dominant gut microbiota that differed significantly among the three groups. Compared to the FMT-DSS group, the relative abundances of *unclassified_Muribaculaceae*, *unclassified_Lachnospiraceae*, and *Lactobacillus* were elevated, while the abundances of *unclassified_Bacillaceae*, *uncultured_proteobacterium*, *Ligilactobacillus* and *Bacteroides* were reduced in the FMT-DSS + SP group (Fig. 5t). Therefore, FMT from mice treated with DSS + SP effectively improved gut microbiota imbalance. Taken together, gut microbiota plays an important and putative role in SP's protection against colitis, hippocampal damage, and anxiety-like disorders.

https://doi.org/10.1038/s41467-025-67904-0

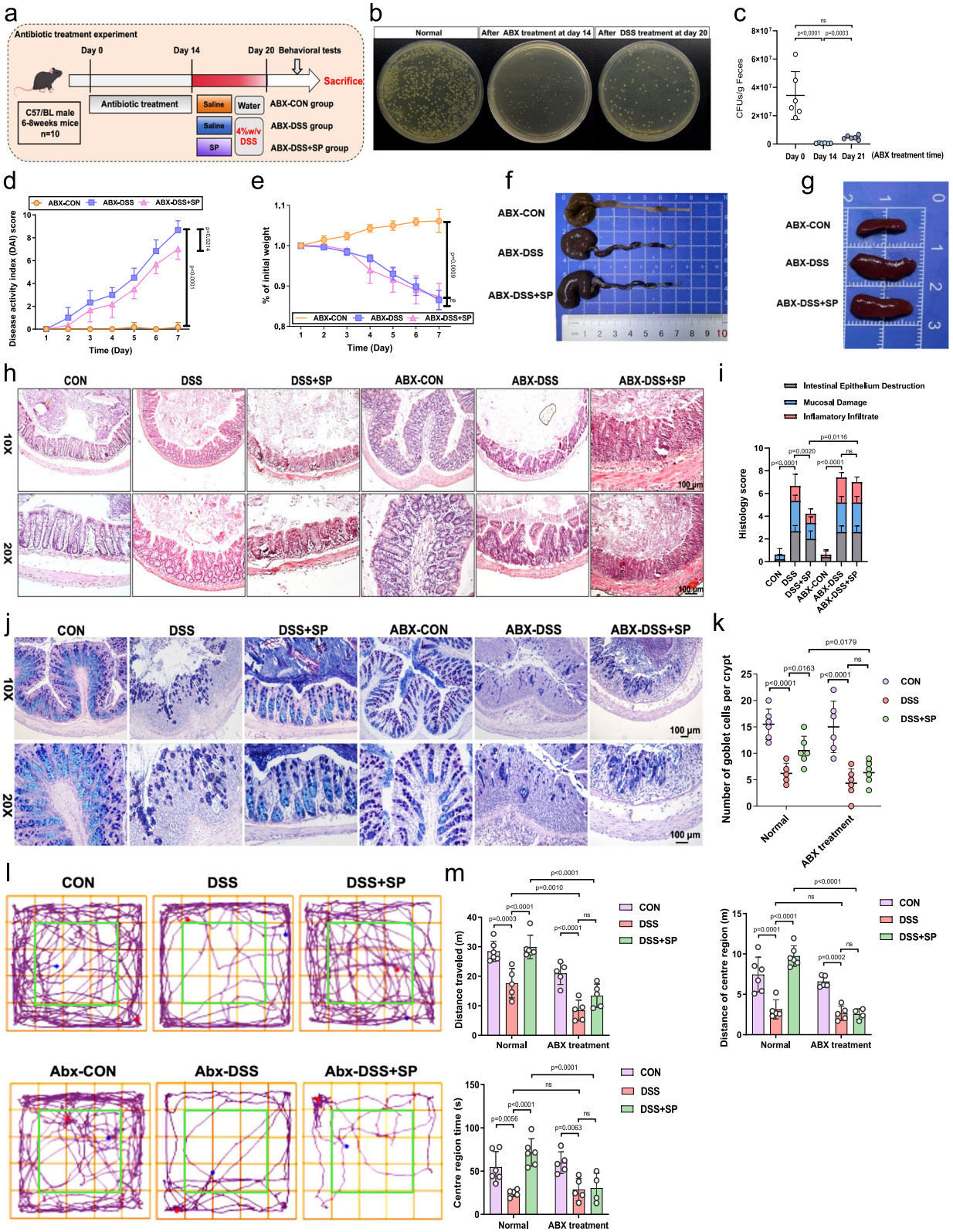

SP affects the expression of hippocampal genes by modulating the gut microbiome, involving the NF-κB and GABAergic/Ca^{2+} signaling pathways

Through modulating the gut microbiome, SP reduces pathological injury and neuroinflammatory responses in the hippocampus, thereby improving anxiety-like behavior, but the potential action mechanism remains unclear. To explore how SP affects the function of the hippocampus mediated via intestinal flora, we performed RNA-seq analysis on the hippocampus of mice subjected to FMT treatment. Principal component analysis (PCA) showed that there were significant differences in the transcriptomes among three groups with four independent replicates (Supplementary Fig. 13a). Compared with the FMT-CON group, 436 differently expressed genes (DEGs) were identified in the FMT-DSS group, of which 271 were upregulated

Fig. 4 | SP protects against intestinal damage and anxiety-like disorders induced by DSS in a gut microbiota-dependent manner. a Schematic diagram of the experimental design (Some schematic elements were created by Figdraw.com). **b**, **c** Comparison of bacterial colony-forming unit (CFU) in feces under LB-aerobic condition. n = 6 mice/group. **d** Disease activity index. n = 6 mice/group. **e** Line diagram showing changes of body weight after ABX treatment. n = 5 mice/group (ABX-CON) and 4 mice/group (ABX-DSS, ABX-DSS + SP). **f** Representative images of the colon. **g** Representative images of spleen. **h**, **i** Representative images of H&E sections and histological scores. Scale bar = 100 μm. n = 5 mice/group. **j**, **k** Representative images of Alcian blue-stained inner mucus layer of colonic sections, and the number of goblet cells per crypt. Scale bar = 100 μm. n = 6 mice/group. **l** Road map of the OFT. **m** Distance traveled, distance of center region, and time spent in the center region. n = 6 mice/group (CON, DSS + SP) and 5 mice/group (the remaining groups). Data were presented as means ± SD. For CFU measurement, one-way ANOVA was performed followed by Tukey's multiple comparisons test, and the rest of the statistics were analyzed using two-way ANOVA. $^{*}P \le 0.05$, $^{**}P \le 0.01$, $^{***}P \le 0.001$. Source data are provided as a Source Data file.

and 165 were downregulated. Furthermore, 387 significantly altered genes were identified in the FMT-DSS + SP *vs.* FMT-DSS groups. Among them, 82 genes were upregulated, and 305 genes were downregulated by FMT-DSS + SP treatment (Supplementary Fig. 13b). A Venn diagram revealed that there were 436 FMT-DSS-regulated DEGs between FMT-DSS and FMT-CON groups, 387 SP-regulated DEGs between FMT-DSS + SP and FMT-DSS groups, and 158 genes that were co-regulated by the treatment of FMT-DSS and FMT-DSS + SP (Supplementary Fig. 13c). The gene expression profile in the hippocampus comparing FMT-DSS to FMT-CON, or comparing FMT-DSS + SP with the FMT-DSS group, were presented in a hierarchical clustered heatmap (Fig. 6a, b). The volcano plot also revealed similar results in the FMT-DSS *vs.* FMT-CON groups and in the FMT-DSS + SP vs. FMT-DSS groups (Supplementary Fig. 13d, e). To gain a deeper understanding of these signaling differences, the Kyoto Encyclopedia of Genes and Genomes (KEGG) pathway analysis was performed. Results showed the notable enrichment in a series of signaling pathways (top 20 enriched), including upregulated or downregulated alterations, in the FMT-DSS *vs* FMT-CON (Fig. 6c, d) as well as in the FMT-DSS + SP *vs* FMT-DSS (Fig. 6e, f). Of note, the NF-κB signaling pathway was activated in the FMT-DSS group, which could be dramatically reversed by FMT-DSS + SP administration. RT-qPCR analysis demonstrated the mRNA expressions of *IKBα* and *p65* were upregulated in the hippocampus of the FMT-DSS group compared to the FMT-CON group, however, treatment with FMT-DSS + SP notably reversed these processes (Fig. 6g). Western blotting analysis demonstrated the NF-κB pathway molecules, including p-p65 and p-IKBα, were upregulated in the hippocampus of the FMT-DSS group compared to the FMT-CON group, however, treatment with FMT-DSS + SP notably reversed these alterations (Fig. 6h and Supplementary Fig. 14a, b).

Remarkably, KEGG pathway analysis also revealed that the neuroactive ligand–receptor interactions and Ca^{2+} signaling pathway were significantly activated in the FMT-DSS + SP group. Among the neuroactive ligand-receptor interactions signaling, ligand-gated channels, such as gamma-aminobutyric acid receptor (GABAR), are permeable for calcium upon activation[42]. Likewise, the mRNA expressions of *Gabra1*, *Gabra3*, *Gabrb2* and *Camk2d* genes were decreased in the FMT-DSS group compared with the FMT-CON group, but FMT-DSS + SP treatment significantly suppressed the reduction of these genes in the hippocampus (no significant change in the *Gabrg2* gene was observed) (Fig. 6i). Consequently, the increased protein expression of $GABA_AR\alpha1$, $GABA_BR2$, GAD65 (a key enzyme responsible for the synthesis of GABA), and CaMKII (a sensor of calcium concentration change) in hippocampus tissues of the FMT-DSS + SP group was further confirmed by western blotting assay (Fig. 6j and Supplementary Fig. 14c-f). Additionally, the UALCAN database was used to investigate the potential involvement of NF-κB pathway and GABAergic/Ca^{2+} signaling in patients with COAD. Our analysis revealed that there was a significant increase in the mRNA levels of key NF-κB-related genes (Supplementary Fig. 15a-e), and the mRNA expressions of genes in the GABAergic/Ca^{2+} signaling pathway were decreased (Supplementary Fig. 15f-l).

Microglia, as key players in the inflammatory signaling process, are associated with the NF-κB signaling pathway, which is crucial for regulating inflammation[43]. Excitingly, SP has been shown to prevent the decrease in the number of astrocytes induced by DSS. Astrocytes are known to perform many important functions that support neurons and maintain brain health[44]. We hypothesized that the effects of FMT treatment on the NF-κB and GABAergic/Ca^{2+} signaling pathways may be closely linked to changes in microglia and astrocytes. To investigate this, we performed double-immunofluorescence staining to test the p-IKBα signaling within $Iba1^+$ microglia in the CA1 and DG regions of the hippocampus. As shown in Fig. 6k and Supplementary Fig. 14g, administration of FMT-DSS significantly increased the number of p-$IKB\alpha^+$ microglia in the hippocampus of mice. In contrast, p-$IKB\alpha^+$ microglia were dramatically lower in the FMT-DSS + SP mice than in the FMT-DSS mice. $GABA_AR\alpha1$ immunoreactivity was observed in astrocytes, and FMT-DSS + SP treatment dramatically elevated the expression of $GABA_AR\alpha1$ within astrocytes (Fig. 6l and Supplementary Fig. 14h). Using double-immunofluorescence staining, the co-localization of the CaMKII with astrocyte marker GFAP was analyzed. Similarly, in alignment with the results of western blotting, the number of $CaMKII^+$ astrocytes was down-regulated in the FMT-DSS group, which could be reversed by FMT-DSS + SP treatment (Fig. 6m and Supplementary Fig. 14i). To gain a more precise understanding of the molecular mechanisms involved in microglia and astrocytes, we isolated these cells from hippocampal tissue by flow cytometry sorting. As illustrated in Supplementary Fig. 16a, microglia were identified as $CD11b^+CD45^{low}$, and astrocytes were identified as $ACSA2^+$. The collected microglia and astrocytes were subjected to separate RNA sequencing analyses. A heatmap depicted the differentially expressed genes in the NF-kappa B signaling pathway in the microglia, revealing that genes enrichment in this pathway was evident from the FMT-DSS group but absent in the FMT-DSS + SP group (Fig. 6n). KEGG pathway analysis of differentially expressed genes showed a downregulation of pro-inflammatory pathways, including the NF-kappa B signaling pathway, the TNF signaling pathway, and cytokine-cytokine receptor interactions, in the microglia of mice treated with FMT-DSS + SP compared to those treated with FMT-DSS (Supplementary Fig. 16b). Gene set enrichment analysis (GSEA) analysis indicated that the gene set associated with the NF-kappa B signaling pathway was significantly down-regulated in the FMT-DSS + SP group compared with FMT-DSS group (Fig. 6n). Additionally, the RNA-Seq analysis of astrocytes from mice treated with FMT-DSS + SP revealed broad enrichment of genes in neuroactive ligand–receptor interaction and calcium signaling pathway compared to those from mice treated with FMT-DSS (Fig. 6o). Notably, KEGG pathway analysis revealed that neuroactive ligand–receptor interaction and GABAergic synapse were significantly enriched in the astrocytes of the FMT-DSS + SP group (Supplementary Fig. 16c). GSEA also revealed a significant down-regulation of the gene set in neuroactive ligand–receptor interaction in the FMT-DSS group compared to the FMT-CON group, however, the FMT-DSS + SP group exhibited an up-regulation of the gene set related to neuroactive ligand-receptor interaction compared to the FMT-DSS group (Fig. 6o).

Overall, these results suggest that the suppression of the NF-κB pathway in microglia, coupled with the activation of GABAergic and downstream Ca^{2+} signaling in astrocytes, is responsible for SP's anti-neuroinflammatory and anti-anxiety activities mediated by the gut microbiota.

https://doi.org/10.1038/s41467-025-67904-0

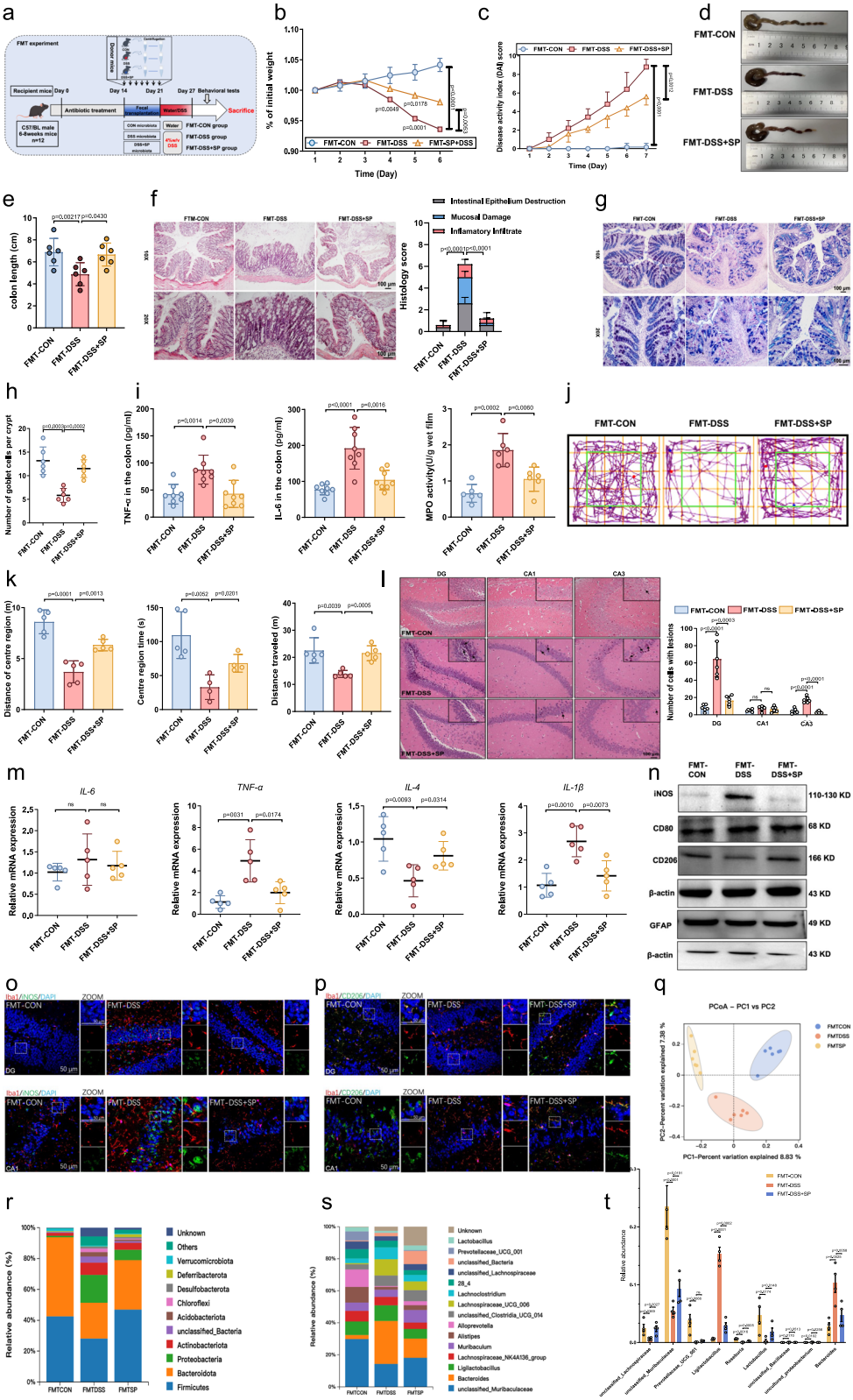

SP augments the enrichment of gut microbiota-derived metabolite inositol

Considering the interplay between the intestinal microbiota and host metabolism, as well as the role of microbiota-derived metabolites in gut-brain communication[45], an untargeted metabolomic analysis was subsequently carried out on samples that had previously undergone 16S rRNA gene sequencing. To further verify the differences among samples from three groups, the score plot of partial least squares discriminant (PLS-DA) analysis was performed. There was an obvious separation among the CON, DSS, and DSS + SP groups, and the DSS + SP group was closer to the CON group than to the DSS group, indicating that SP significantly mitigated DSS-induced dramatic alteration of metabolites (Fig. 7a). A total of 980 metabolites were identified in the DSS and CON groups, whereas 395 metabolites were identified in

Fig. 5 | The FMT experiment reveals that SP attenuates colitis and anxiety-like behavior induced by DSS through modulating the gut microbiota. a Schematic illustration of experimental design (Some schematic elements were created by Figdraw.com). **b** Body weight change. n = 5 mice/group. **c** Disease activity index. n = 5 mice/group. **d**, **e** Representative images and colon length. n = 6 mice/group. **f** Representative images of H&E staining of colon tissues of each group. Scale bar = 100 μm. n = 5 mice/group. **g, h** AB-PAS staining of the murine colon, and the number of goblet cells per crypt. Scale bar = 100 μm. n = 6 mice/group. **i** Determination of IL-6 (n = 8 mice/group) and TNF-α (n = 8 mice/group) levels by ELISA in the colon, and MPO activity (n = 6 mice/group). **j** Representative traces during the 5 min OFT. **k** Distance of center region, n = 5 mice/group, center area time spent, n = 5 mice/group (FMT-CON) and 4 mice/group (FMT-DSS, FMT-DSS + SP) and total distance traveled, n = 5 mice/group. **l** Representative images of H&E-staining for the hippocampus sections and quantitative analysis. Scale bar = 100 μm. n = 6 mice/group. **m** RT-qPCR assay of inflammatory cytokines (*IL-6*, *TNF-α*, *IL-4* and *IL-1β*) in the hippocampus. n = 5 mice/group. **n** Imaging of western blots showing that relative protein expression of iNOS, CD80, CD206, GFAP and β-actin in the hippocampus of mice. n = 3 independent experiments. **o** Double immunofluorescence staining for Iba-1 (red)/iNOS (green) in CA1 and DG regions of the hippocampus and statistical analysis. Scale bar = 50 μm. n = 3 independent experiments. **p** Representative immunofluorescence images of double-labeling for Iba-1 (red) and CD206 (green) in hippocampus tissues, and statistical analysis. Scale bar = 50 μm. n = 3 independent experiments. **q** Principal coordinates analysis (PCoA) of gut microbial based on the binary Jaccard distance. n = 6 mice/group. **r** Taxonomic distributions of gut bacterial composition at the phylum level. n = 6 mice/group. **s** Taxonomic distributions of gut bacterial composition at the genus level. n = 6 mice/group. **t** ANOVA result shows the relative abundance of the dominant gut microbiota at the genus level in each group. n = 4 mice/group. Data were presented as means ± SD. For DAI score and body weight change, two-way repeated-measures ANOVA was performed and the rest of the statistics was analyzed using one-way ANOVA followed by Tukey's multiple comparisons test. $^{*}P \le 0.05$, $^{**}P \le 0.01$, $^{***}P \le 0.001$. Source data are provided as a Source Data file.

the DSS + SP and DSS groups. A total of 144 metabolites were identified in the three groups (Fig. 7b). The results of volcano plot showed that compared to the CON group, 352 metabolites were up-regulated and 628 down-regulated in the DSS group. However, 215 metabolites were increased, and 180 metabolites declined in the DSS + SP group vs the DSS group in mouse colonic contents (Fig. 7c, d).

KEGG pathway enrichment of the differential metabolites showed that Amino acid metabolism (Arginine and proline metabolism, and Cysteine and methionine metabolism), Biosynthesis of other secondary metabolites (Neomycin, Kanamycin and gentamicin biosynthesis, Betalain biosynthesis, Biosynthesis of various antibiotics and Caffeine metabolism) and Carbohydrate metabolism (Ascorbate and aldarate metabolism, Amino sugar and nucleotide sugar matabolism, Galactose metabolism and Inositol phosphate metabolism) were the main pathways based on KEGG analysis (Fig. 7e). Specifically, heatmap analysis was performed to observe the relative expression of these differentially expressed metabolites in the three groups; the top five most abundant metabolites in the DSS + SP group, compared with the DSS group included myo-Inositol, 6-O-Methylguannine, Threoninyl-Gamma-glutamate, Diplodiatoxin, and Tacrine (Fig. 7f). Enrichment analysis of the elevated metabolites in the DSS + SP group was conducted through KEGG database. Data indicated that Inositol phosphate metabolism, O-Antigen nucleotide sugar biosynthesis, Galactose metabolism, Vitamin B6 metabolism and Pentose and glucuronate interconversions were the top five enrichment pathways, and of these, inositol phosphate metabolism was remarkably changed (Fig. 7g). Notably, we further identified and screened some evidently changed metabolites in the DSS + SP group *vs* the DSS group, as shown in Fig. 7h, i. Among them, N-oleoyl GABA and tacrine were enriched in the biosynthesis of neurochemicals. In particular, inositol was the most significantly increased metabolite in colonic contents in response to SP administration, and was enriched in a variety of metabolic processes, involving biosynthesis of antibiotics, inositol phosphate metabolism, ascorbate and aldarate metabolism, and galactose metabolism. The above results reveal that the administration of SP enhanced microbiota-derived metabolite production, particularly inositol, indicating that metabolites might be involved in the SP-mediated protection against colitis and anxiety-like behaviors induced by DSS.

Administration of inositol ameliorates DSS-induced colitis and anxiety-like disorders

To verify the protective effects of inositol, which was a highly generated metabolite in the DSS + SP group, we administered inositol to the mice in drinking water (Fig. 8a). Supplementation with inositol potently repressed the weight loss and DAI induced by colitis (Fig. 8b, c). The colon length dramatically declined in the DSS group compared to the CON group, and this downregulation was repressed by inositol supplementation (Supplementary Fig. 17a). Histological examination revealed that DSS-induced reductions in crypt depth, as well as damage or exfoliation of epithelial cells, were substantially ameliorated following inositol treatment (Fig. 8e and Supplementary Fig. 17b), as indicated by lower histological scores (Supplementary Fig. 17c). A deficiency of E-cadherin in the mouse intestinal epithelium worsens the clinical symptoms and histological characteristics of colitis induced by DSS[46]. Therefore, we performed immunofluorescent staining for E-cadherin and observed a severe loss of E-cadherin in DSS-treated mice. However, inositol potently restored E-cadherin expression during colitis, suggesting that inositol could protect intestinal epithelial cells from breakdown induced by DSS (Fig. 8f and Supplementary Fig. 17d). To further, we found that the mRNA expressions of *IL-1β*, *IL-6*, and *TNF-α* were strikingly decreased in the colon tissues of inositol-treated mice compared with those of DSS-treated mice (Fig. 8g). It is noteworthy that no significant differences in weight loss, DAI, colon length, and pathological changes were observed between the group treated with inositol alone and the CON groups.

The protective effects of inositol on anxious-like behaviors were evaluated by OFT, and EPM assays. As shown in Fig. 8h, i, the results of OFT demonstrated that DSS-treated mice exhibited a shorter path length, less distance of center region and lower movement speed. On the contrary, inositol supplementation evidently mitigated these behavioral abnormalities induced by colitis. We then examined the effect of inositol in the EPM test (Fig. 8j, k). Compared to the DSS group, behavioral symptoms improved in the DSS+inositol group, which exhibited an obvious increase in the percentage of time spent in the open arms and percentage of times entering the open arms. Mice treated with inositol also exhibited a higher total distance traveled than DSS-treated mice (Supplementary Fig. 18). Notably, the differences in behavioral tests between the CON group and the inositol alone group did not reach statistical significance. As shown in Fig. 8l and Supplementary Fig. 17e, in the DG region, hippocampal cells were clearly and uniformly stained and neatly arranged in the CON group. Compared with the CON group, the DSS group exhibited loosely arranged cells and obvious nuclear consolidation. However, in the DSS +inositol group, the number of cells was augmented, and nuclear condensation was significantly improved. Remarkably, no significant alterations in hippocampal pathology were detected in the inositol alone group compared to the CON group. Besides, Nissl staining results confirmed that following inositol treatment, DSS-induced pathological changes in the hippocampal DG region, such as the reduction of Nissl bodies, pyknosis, and neuronal shrinkage, were notably restored (Fig. 8m and Supplementary Fig. 17f). To demonstrate whether inositol treatment played a significant role in mitigating neuroinflammation, RT-qPCR assay revealed that DSS intervention increased mRNA expression of the pro-inflammatory factor *IL-6*, *IL-1β*, and *TNF-α* in the hippocampus, which was reversed by inositol supplementation. Meanwhile, inositol elevated anti-inflammatory factor

https://doi.org/10.1038/s41467-025-67904-0

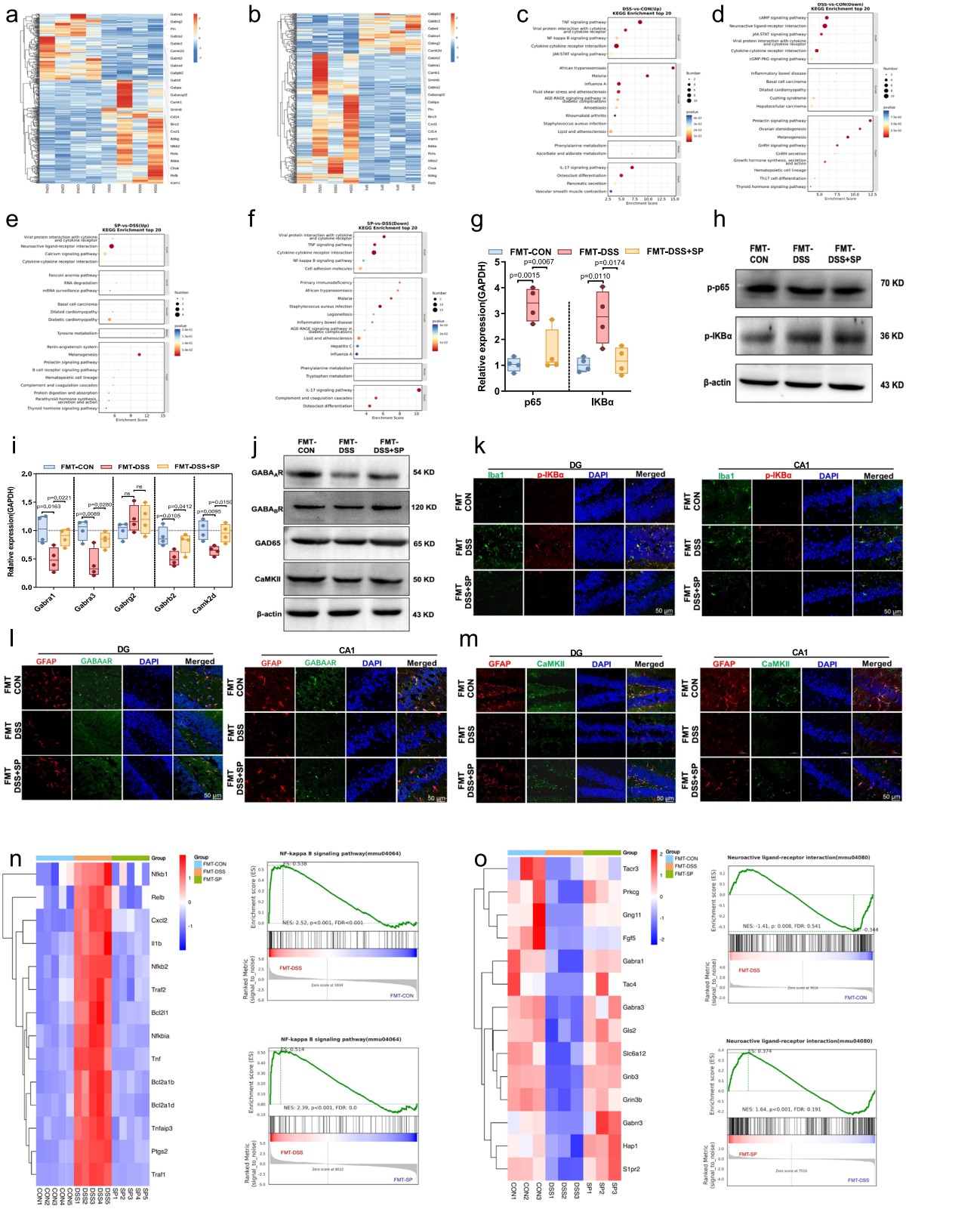

IL-10 mRNA expression (Fig. 8n). We then investigated whether inositol administration affected the activation of microglia. Results of immunohistochemical staining revealed that an up-regulated area of Iba-1 positive cells was observed in the DSS group compared to the CON group in the hippocampal DG and CA1 regions; however, inositol supplementation dramatically diminished the percentage of Iba-1$^+$ cells (Fig. 8o, and Supplementary Fig. 17g).

A previous study reported that inositol undergoes oxidation to fructose and a series of enzymatic reactions to L-glutamate, which is then catalyzed by GAD to produce GABA[47]. We supposed that inositol may improve anxiety-like behavior by promoting GABA synthesis. To verify this conjecture, we detected the content of GABA in the hippocampus by ELISA. In the DSS-induced mice, there was a marked reduction in the concentration of GABA in the hippocampus, in

Fig. 6 | SP affects the expression of hippocampal genes by modulating the gut microbiome, involving the NF-κB and GABAergic/Ca^{2+} signaling pathways. **a**, **b** Heat maps revealing differential gene expression in FMT-DSS *vs* FMT-CON, FMT-DSS + SP vs FMT-DSS groups. n = 4 mice/group. The pathway-related genes were selected (log2 fold change at least > 1, $p < 0.05$). **c**, **d** KEGG analysis of total-, up- and down-regulated genes in the FMT-DSS group compared with the FMT-CON group (Top 20). n = 4 mice/group. **e**, **f** KEGG analysis of total-, up- and down-regulated genes in the FMT-DSS + SP group *vs* the FMT-DSS group (Top 20). n = 4 mice/group. **g** Quantitative real-time PCR analysis of mRNA expressions of NF-κB signaling pathway genes (*p65* and *IKBα*) in the hippocampus. n = 4 mice/group. The whiskers indicate the minimum and maximum values observed within the range of Q1 − 1.5 × IQR to Q3 + 1.5 × IQR. The box reveals the interquartile range (IQR) between the 25th (Q1) and 75th (Q3) percentiles, and the line inside the box represents the median (50th percentile). **h** The protein expression of p-p65 and p-IKBα in hippocampus tissue, as determined by western blotting. n = 3 independent experiments. **i** Quantitative real-time PCR analysis of mRNA expressions of GABA receptor and Ca^{2+} signaling genes (*Gabra1*, *Gabra3*, *Gabrg2*, *Gabrb2* and *Camk2d*). n = 4 mice/group. The whiskers indicate the minimum and maximum values observed within the range of Q1 − 1.5 × IQR to Q3 + 1.5 × IQR. The box reveals the interquartile range (IQR) between the 25th (Q1) and 75th (Q3) percentiles, and the line inside the box represents the median (50th percentile). **j** Protein expressions of $GABA_AR$, $GABA_BR$, GAD65 and CaMKII were measured in hippocampus tissue by western blot. n = 3 independent experiments. **k** Representative immunofluorescence images of double-labeling for p-IKBα (red)/Iba1 (green) in hippocampus tissues. Scale bar = 50 μm. n = 3 independent experiments. **l** Representative immunofluorescence images of double-labeling for $GABA_AR$ (green)/GFAP (red) in hippocampus tissues. Scale bar = 50 μm. n = 3 independent experiments. **m** Double immunofluorescence staining for CaMKII (green)/GFAP (red) in hippocampus tissues and statistical analysis. Scale bar = 50 μm. n = 3 independent experiments. **n** Differential gene expressions were presented by the heatmap in microglia of three groups, and GSEA analysis of microglia from FMT-DSS + SP group vs the FMT-DSS group. n = 4 mice/group. **o** Heat maps of differential gene expression in astrocytes from three groups and GSEA analysis of astrocytes from FMT-DSS + SP group vs the FMT-DSS group. *n* = 4 mice/group. Data were presented as means ± SD. Statistical significance was determined using one-way ANOVA followed by Tukey's multiple comparisons test. $^*P \le 0.05$, $^{**}P \le 0.01$, $^{***}P \le 0.001$. Source data are provided as a Source Data file.

contrast, the GABA level was appreciably enhanced following supplementation with inositol (Fig. 8p). To further evaluate the effect of inositol on GABA signaling, the expression of two GABA receptor subunits (*$GABA_AR\alpha1$* and $GABA_BR2$) was assayed in the hippocampus. Interestingly, they were both significantly up-regulated after inositol supplementation (Fig. 8q, r and Supplementary Fig. 17h). The activity of GABA at the synapse is terminated by reuptake into nerve terminals and astrocytes, mediated by membrane-bound GABA transporters (GATs), which thereby modulate GABAergic neurotransmission[48]. With that in mind, we performed immunofluorescence staining for GABA transporters1 (GAT1) and GFAP. As depicted in Fig. 8s and Supplementary Fig. 17i, the large processes of GFAP-immunopositive astrocytes were encompassed by the GAT1-expressing area in DG and CA1 regions, and the merged images showed occasional co-localization of GAT1- and GFAP-immunostaining. It's worth noting that the number of $GFAP^+$ astrocytes was dramatically reduced after DSS treatment, which could be overturned by inositol supplementation. In addition, the density of $GAT1^+$ astrocytes appeared to be higher in the DSS+inositol group compared to the DSS group. Interestingly, no apparent intestinal pathological and behavioral alterations were observed in the inositol alone group, compared to the CON group. Collectively, these data suggest that inositol might serve as a critical candidate metabolite associated with the beneficial effects exerted by SP.

Inositol plays an essential role in the action of SP against anxious-like behaviors in DSS-induced mice

To next assess whether inositol is required for the positive effects of SP on anxiety-like symptoms, we treated mice with the inositol synthesis inhibitor, L-690330 (Fig. 9a). Behavioral analysis indicated that the anti-anxiety effects of SP were reversed by L-690330 treatment. Specifically, in the EPM test, colitis mice treated with both SP and L-690330 showed decreased percentage of time spent and distance traveled in the open arms, as well as lower percentage of times entering the open arms and total distance traveled, compared to SP-treated colitis mice (Fig. 9b, c and Supplementary Fig. 19a). In the EZM test, following L-690330 treatment, both the percentage of time spent in the open zones and the percentage of times entering the open zones were significantly reduced relative to SP-treated colitis mice (Fig. 9d, e). Although the total distance traveled showed a decreasing trend, this change was not statistically significant (Supplementary Fig. 19b). In the LDB test, colitis mice treated with SP and L-690330 exhibited lower percentages of time spent in the light box, distance traveled in the light box and total distance traveled, compared to those treated with SP alone (Fig. 9f and Supplementary Fig. 19c). However, no differences were observed in the transition frequencies between the light and dark chambers among the three groups. To evaluate microscopic variations in the hippocampus, we stained hippocampal sections with H&E (Fig. 9g and Supplementary Fig. 20a). Representative images revealed that the administration of SP repaired DSS-induced pathological characteristics, including shrunken nerve cells, pyknotic or indistinct nuclei, and an increase in injured neurons in the DG region. Intriguingly, L-690330 treatment markedly reversed the protective influence of SP on the hippocampus. Additionally, no statistical differences were observed in the CA1 and CA3 regions among the three groups. We further investigated the impact of inositol inhibition on neuronal survival in the DG region using Nissl staining. SP mitigated the loss of Nissl bodies, pyknotic and indistinct nuclei in the DG region, resulting in a significant increase in the number of surviving neurons. However, the administration of L-690330 effectively reversed these changes (Fig. 9h and Supplementary Fig. 20b). These findings substantiate the role of inositol in the neuroprotective properties of SP.

In light of the important role of inositol, we detected whether inositol level increased following FMT from DSS + SP-treated mice using ELISA. As expected, the concentration of inositol in the hippocampus of the FMT-DSS group was markedly lower than that in the FMT-CON group. However, a significant upregulation of inositol was detected in the FMT-DSS + SP group in comparison with the FMT-DSS group (Fig. 9i). Similar trends were observed in the serum (Fig. 9j). Given the substantial increase in inositol concentration in both the hippocampus and serum following FMT from DSS + SP-treated mice, we hypothesized that inositol might exert a direct impact on the brain. To investigate this, we assessed the functional activity of inositol by culturing mouse microglial cell line (BV-2) and mouse astrocyte cell line (C8D1A) in vitro. BV-2 cells were stimulated with LPS at a concentration of 1 μg/mL to mimic a neuroinflammatory environment. Cytotoxicity of inositol was evaluated using a CCK-8 assay. As shown in Supplementary Fig. 21a, BV-2 cells treated with different concentrations of inositol (25, 50, and 100 μM) for 24 h exhibited no discernible cytotoxic effects. Further RT-qPCR analysis indicated that mRNA levels of *TNF-α*, *IL-1β*, and *IL-6* were down-regulated at concentrations of 25 and 50 μM in the inositol groups, although these levels were not significantly different from those observed in the LPS group (Fig. 9k-m). Importantly, treatment with 100 μM inositol significantly reduced the levels of these inflammatory mediators. Additionally, the mRNA expression of *iNOS* in all inositol groups was lower than that observed in the LPS group, although no statistically significant differences were noted (Fig. 9n). Meanwhile, C8D1A cells were cultured with inositol for 24 h. The results revealed that inositol exhibited no significant toxicity to C8D1A cells at concentrations of 50, 100 and 200 μM (Supplementary Fig. 21b). Subsequently, C8D1A cells were treated with

https://doi.org/10.1038/s41467-025-67904-0

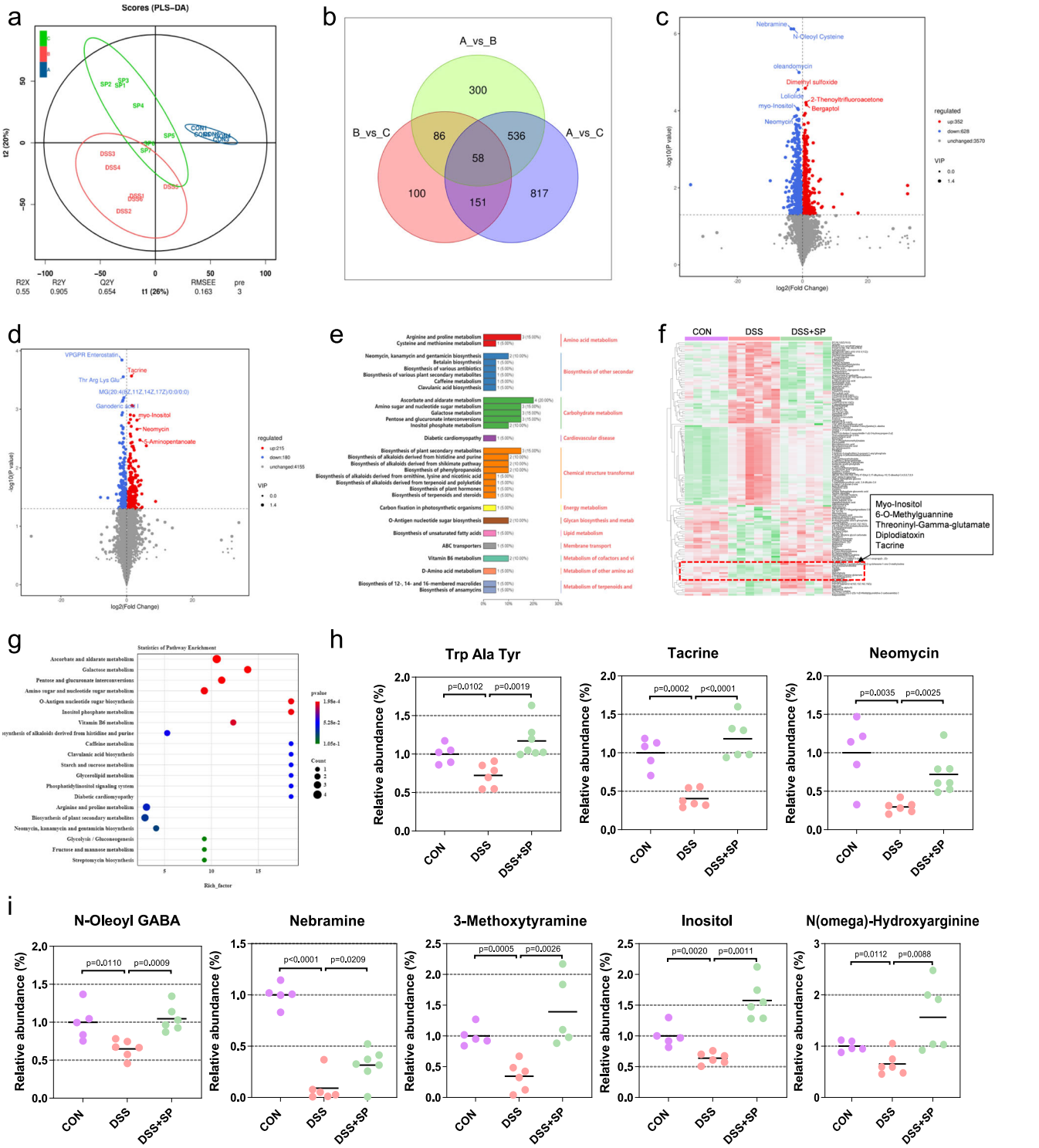

Fig. 7 | SP augments the enrichment of gut microbiota-derived metabolite inositol. a PLS-DA of metabolomic profiles in colonic contents. **b** Differentially expressed metabolites were identified by Venn diagram. **c** The analysis of volcano plots in the DSS group *vs* the CON group, and **d** in the DSS group *vs* the CON group. **e** Enrichment analysis of metabolites through KEGG pathway analysis in the CON, DSS and DSS + SP groups. **f** Heat map of significantly altered metabolites in colonic contents of mice. Metabolites with the Variable importance in the projection (VIP) value of PLS-DA model >1 and the *P* values of two-tailed Student's *t* test <0.05 were considered to be significantly different. **g** The enriched pathways analysis of the differential metabolites in the DSS + SP group. The x-axis represents the pathway impact, and the y-axis represents the pathway enrichment. **h**, **i** Concentrations of amino acid, tacrine, neomycin, N(omega)-hydroxyarginine, N-oleoyl GABA, inositol, nebramine, gamma-glutamyl-L-putrescine and 3-methoxytyamine in the colonic contents of mice. n = 6 mice/group. Data were presented as means ± SD. Statistical significance was determined using one-way ANOVA followed by Tukey's multiple comparisons test (**h**, **i**). $^{*}P \le 0.05$, $^{**}P \le 0.01$, $^{***}P \le 0.001$. Source data are provided as a Source Data file.

https://doi.org/10.1038/s41467-025-67904-0

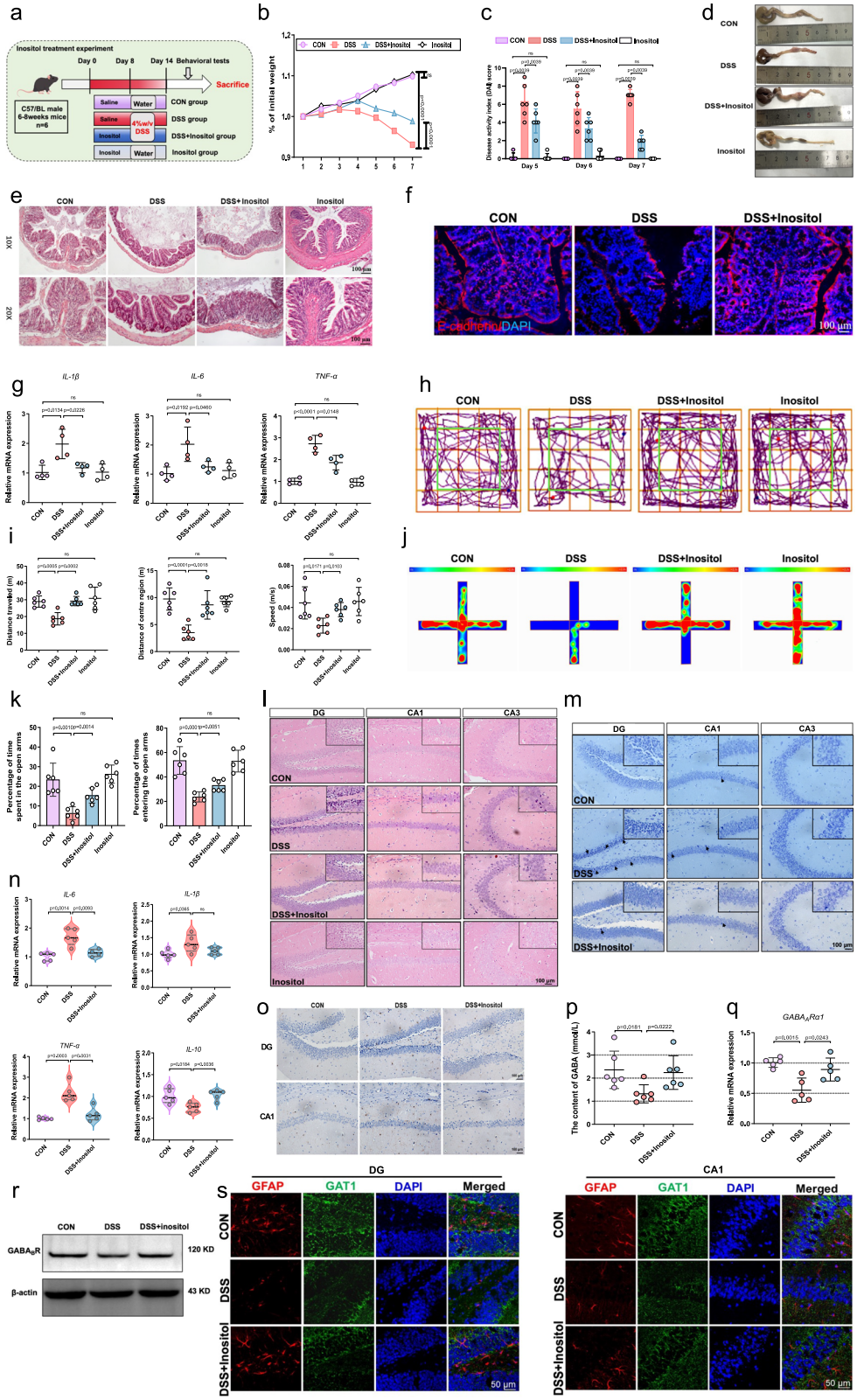

inositol under stimulation of LPS for 24 h. Compared to the LPS exposure alone, inositol treatment increased the mRNA levels of *Gabra3* and *Camk2d*, with the most pronounced effects observed at a concentration of 200 μM (Fig. 9o, p). Consistent with these findings, western blot analysis illustrated that LPS exposure reduced the protein expression of $GABA_AR1$, CaMKII and $GABA_BR$ in C8D1A cells. In contrast, supplementation with inositol at both 100 and 200 μM markedly suppressed the downregulation of these protein expressions (Fig. 9q and Supplementary Fig. 21c). The above results suggest that inositol, as a crucial intermediate metabolite, plays an important role in the protective effects of SP against DSS-induced anxiety-like behavioral disorders by enhancing GABAergic neurotransmission signaling in astrocytes and modulating neuroinflammatory responses triggered by activated microglia.

Fig. 8 | Gut metabolite inositol mediates the protective effects of SP against colitis and anxious behaviors in DSS-induced mice. a Diagram illustrating the mouse model of colitis employed in this study, and inositol treatments are indicated (Some schematic elements were created by Figdraw.com). **b** Daily body weight changes. n = 8 mice/group. **c** Diseases activity index. n = 6 mice/group. **d** Macroscopic pictures of colons. **e** H&E-stained colon sections. Scale bar = 100 μm. n = 5 independent experiments. **f** Immunofluorescence staining for E-cadherin (red)/DAPI (blue) in colon tissues. Scale bar = 100 μm. n = 4 independent experiments. **g** The mRNA level of inflammatory cytokines (*IL-1β*, *IL-6* and *TNF-α*) in the colon. n = 4 mice/group. **h**, **i** Representative movement tracks in the open field test and related bar graphs (Distance traveled, distance of center region and speed). n = 6 mice/group. **j**, **k** Track plot of the elevated plus maze, and statistical analysis including percentage of time spent in the open arms and percentage of times entering the open arms. n = 6 mice/group. **l** Representative H&E-stained hippocampus sections of three groups. Scale bar = 100 μm. n = 6 independent experiments. **m** Photomicrographs of Nissl staining in the hippocampus. Scale bar = 100 μm. n = 6 independent experiments. **n** The mRNA expressions of downstream cytokines (*IL-6*, *IL-1β*, *TNF-α* and *IL-10*) in the hippocampus tissue. n = 5 mice/group. **o** Representative immunohistochemistry images of Iba-1 in hippocampus, Scale bar = 100 μm. n = 3 independent experiments. **p** The concentration of GABA in hippocampus tissue. n = 6 mice/group. **q** The mRNA expression of $GABA_AR\alpha1$ in hippocampus. n = 5 mice/group. **r** The protein level of $GABA_BR$ detected by western blot. n = 3 independent experiments. **s** Double immunofluorescence staining for GFAP (red)/GAT1 (green) in the DG and CA1 regions of hippocampus tissue. Scale bar = 50 μm. n = 3 independent experiments. Data were presented as means ± SD. For body weight change, two-way repeated-measures ANOVA was performed and the rest of the statistics was analyzed using one-way ANOVA followed by Tukey's multiple comparisons test. $^*P \le 0.05$, $^{**}P \le 0.01$, $^{***}P \le 0.001$. Source data are provided as a Source Data file.

Multi-omics integration analysis for the connections among the host phenotypes, gut microbiome, metabolites, and brain gene transcription

To identify the influences of the gut microbiome on metabolites in the intestine, the gut microbiome and metabolites were subjected to Spearman's correlation conjoint analysis. *Oscillibacter*, *Romboutsia*, *Enterobacter*, *Clostridioides*, *Butyricimonas*, *Coprobacillus*, *Prevotellaceae_UCG_001*, *Muribaculum*, and *Roseburia* were the key bacteria related to the secretion of metabolites. Importantly, the myo-Inositol was influenced by bacteria involving *Prevotellaceae_UCG_001*, *Oscillospiraceae* and *Azospirillum_sp._47_25* (Supplementary Fig. 22a). Additionally, Spearman's correlations analysis identified the interact among gut bacteria, which then impacted host phenotypes. We found that g_*unclassified_Clostridia_UCG_014*, g_*unclassified_Muribaculaceae*, g_*unclassified_Lachnospiraceae*, g_*Prevotellaceae_UCG_001* and p_*Firmicutes* showed a negative correlation with DAI and pathology score but showed a positive correlation with colon length and MUC-2. The g_*Bacteroides*, g_*Escherichia_Shigella* and p_*Bacteroides* exhibited a positive connection with DAI and pathology score, while a negative correlation was observed with colon length and MUC-2 (Supplementary Fig. 22b). To further investigate the relationship between gut microbiome-derived metabolites and host phenotypes, we conducted Spearman's correlation analysis revealed that the interact among metabolites, including Tacrine, Neomycin, myo-Inositol, 5-Aminopentanoate, N(omega)-Hydroxyarginine, N-Oleoyl GABA, Nebramine, Trp Ala Tyr, 3-Methoxytyramine, Gamma-glutamyl-L-putrescine and 4-Pyridoxate. Furthermore, we observed that myo-Inositol were negatively correlated with host phenotypes (DAI and pathology score), while were positively correlated with host phenotypes (colon length and MUC-2) (Supplementary Fig. 22c). There was a correlation between the gene transcription of the hippocampus and brain phenotypes which included hippocampal inflammatory factor levels, and anxiety-like behaviors (Supplementary Fig. 22d). We found that changes in hippocampal gene transcription in mice are influenced by the gut microbiome (Supplementary Fig. 22e). Specifically, *unclassified_Muribaculaceae*, *unclassified_Lachnospiraceae*, and *Prevotellaceae_UCG_001* showed the capacity of inhibiting the gene expression of NF-κB pathway (*Ikbke*, *Relb*, *Birc3* and *Nfkb2*) and augmenting GABAergic (*Gabarapl2*, *Gabrb2* and *Gabra2*) and Ca^{2+} signaling (*Pin* and *Smim6*), respectively. Whereas a negative correlation was observed with *Escherichia_Shigella* and *Gabarapl2*, *Pin* and *Smim6*. To further, combined data analyses of network interaction showed associations among host phenotypes, brain phenotypes, DEGs, luminal metabolites, and gut microbiota in Supplementary Fig. 22f ($|R| > 0.50$, $P < 0.05$). Spearman's correlations revealed positive correlations between anxiety-like behaviors and the gene expression of the NF-κB pathway (*Cxcl1*, *Nfkb2*, *Rela*, *Relb*, *Chuk*, *Ikbkg* and *Ikbke*), while there were negative correlations between anxiety-like behaviors and the expression of GABAergic signaling genes (*Gabra2*, *Gabrb2*, *Gabra1*, *Gabpb2*, *Gabbr2*, and *Gabarapl2*) and Ca^{2+} signaling genes (*Pin*, *Smim6*, *Camk2d* and *Camk1*). Likewise, the expression of hippocampal inflammatory factors was negatively correlated with the expression of GABAergic and Ca^{2+} signaling genes, while positively correlated with the expression of NF-κB pathway genes. Inositol showed negative correlations with the expression of the NF-κB pathway genes (*Ikbke*, *Ikbkg*, *Nfkb2* and *Relb*) and exhibited positive correlations with the expression of GABAergic signaling genes (*Gabrb2*, *Gabarapl2*, *Gabbr2*) and Ca^{2+} signaling genes (*Smim6* and *Camk1*).

Protective effects of SP on clinical symptoms and macroscopic tissue damage in TNBS-induced colitis

Ultimately, we conducted a preliminary exploration of the effects of SP in a 2,4,6-Trinitrobenzenesulfonic acid (TNBS)-induced mouse model, which is known to replicate some features of Crohn's disease with transmural inflammation[49]. The experimental design was revealed in Supplementary Fig. 23a. The results showed that on day 7, mice treated with TNBS exhibited significant weight loss compared to the CON group, whereas administration of SP, at both low and high doses, significantly mitigated the weight loss induced by TNBS (Supplementary Fig. 23b). The DAI was utilized to assess the severity of colitis symptoms[50]. Mice treated with SP at both doses showed lower DAI compared to the TNBS group (Supplementary Fig. 23c). Colon shortening is a key indicator of the severity of TNBS-challenged colitis[51], and we observed a significant restoration of colon length following SP administration (Supplementary Fig. 23d). Furthermore, pathological features of colitis were evaluated through H&E staining. As shown in Supplementary Fig. 23e, f, the TNBS group demonstrated significant increases in crypt cell loss, submucosal edema, inflammation (mononuclear cell infiltration), ulcers, and hemorrhage compared to the CON group. Notably, SP markedly improved mucosal architecture and overall pathological indices in mice with TNBS-induced colitis. Histological scores corroborated these findings (Supplementary Fig. 23g), with the TNBS group exhibiting significantly higher scores compared to the CON group. Conversely, SP (both low and high dose) significantly reduced the histological scores. Although the high-dose SP group exhibited a greater ameliorative effect, no statistically significant difference was observed.

To assess TNBS-induced anxiety-like behaviors in mice and evaluate the corresponding therapeutic effects of SP, we conducted behavioral tests. In the OFT (Supplementary Fig. 23h, i), parameters such as mean speed, distance of the center region, and time spent in the central region were significantly lower in the TNBS-treated group compared to the CON group. Notably, SP administration at a dose of 5 nmol/kg significantly increased mean speed; however, the changes in distance of the center region and time duration in the central region at this dose were not statistically significant compared to the TNBS group. Conversely, SP at dosages of 10 nmol/kg markedly enhanced mean speed, distance and time spent in central areas compared to the

https://doi.org/10.1038/s41467-025-67904-0

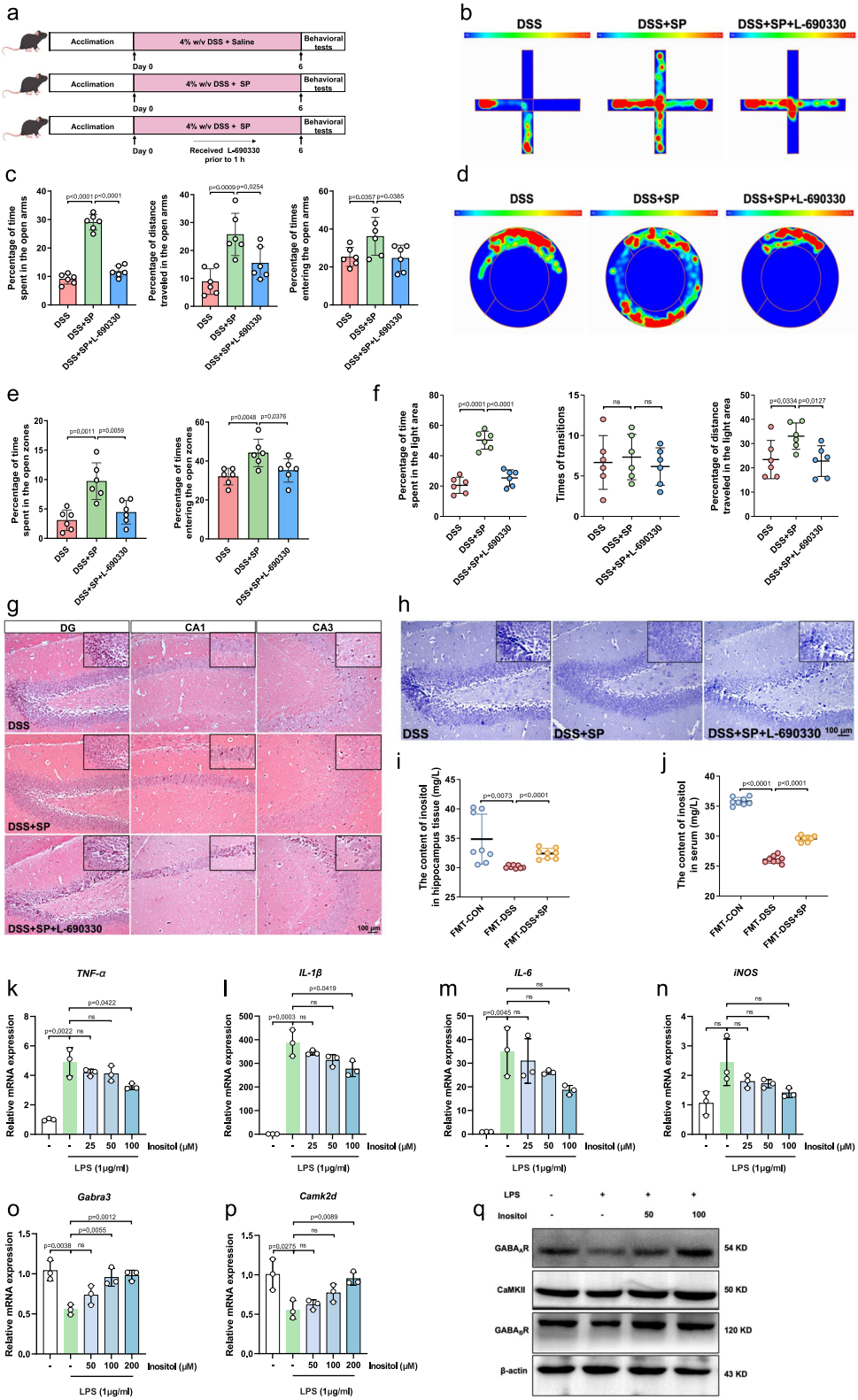

TNBS-treated mice. In the EPM test, the TNBS group exhibited reduced times entering the open arms, lower distance traveled and time spent in the open arms and total distance traveled. However, these behavioral characteristics were mitigated following administration of SP at dosages of 5 and 10 nmol/kg (Supplementary Fig. 23j, k). Next, we performed H&E staining to evaluate TNBS-induced pathological damage in the hippocampus and the effects of SP treatment. As shown in Supplementary Fig. 23l, m, the DG region of the hippocampus in the CON group exhibited normal tissue morphology, characterized by intact nuclei and abundant cytoplasm. In contrast, TNBS treatment resulted in significant neuronal atrophy, nuclear pyknosis, and uneven cytoplasmic staining. However, the administration of SP significantly alleviated these pathological changes induced by TNBS. These results suggest that SP could improve TNBS-

Fig. 9 | Inositol plays an essential role in the action of SP against anxious-like behaviors in DSS-induced mice. a Schematic illustration of experimental design (Some schematic elements were created by Figdraw.com). **b**, **c** Track plot of the elevated plus maze, and statistical analysis including percentage of time spent in the open arms, percentage of distance traveled in the open arms and percentage of times entering the open arms. n = 6 mice/group. **d**, **e** Track plot of the elevated zero maze, and statistical analysis including percentage of time spent in the open zones and percentage of times entering the open zones. n = 6 mice/group. **f** Statistical analysis, including percentage of distance traveled in the light area, percentage of time spent in the light area, and times of transitions in the light-dark box test. n = 6 mice/group. **g** Representative images of H&E-staining for the hippocampus sections. Scale bar = 100 μm. n = 6 independent experiments. **h** Representative images of Nissl staining for the hippocampus sections. Scale bar = 100 μm. n = 4 independent experiments. **i** The content of inositol in hippocampus tissue tested by ELISA. n = 8 mice/group. **j** The content of inositol in serum tested by ELISA. n = 8 mice/group. **k**–**n** The mRNA expression of *TNF-α*, *IL-1β*, *IL-6* and *iNOS* in BV-2 cells. n = 3 mice/group. **o, p** The mRNA expression of *Gabra3* and *Camk2d* in C8D1A cells. n = 3 mice/group. **q** The protein level of $GABA_AR$, CaMKII, $GABA_BR$ detected by western blot. n = 3 independent experiments. Data were presented as means ± SD. Statistical significance was determined using one-way ANOVA followed by Tukey's multiple comparisons test. $^*P \le 0.05$, $^{**}P \le 0.01$, $^{***}P \le 0.001$. Source data are provided as a Source Data file.

induced anxiety-like behaviors and hippocampal tissue injury induced by TNBS.

Discussion

Our work has investigated the therapeutic effects of SP on IBD-like symptoms and behavioral disorders, focusing on the microbiota-gut-brain axis. SP reduced colitis by preserving the intestinal barrier integrity and ameliorated anxiety-like disorders via suppressing pathological changes and neuroinflammation in the hippocampus of DSS-treated mice. These beneficial effects of SP were achieved by modulating the gut microbiome composition and subsequently upregulating the production of microbiota-derived metabolite, inositol, implying an intestinal flora-dependent mechanism. Furthermore, the antianxiety activities of SP were attributable to the suppression of the NF-κB signaling pathway in microglia as well as the activation of GABAergic neurotransmission and downstream Ca^{2+} signaling within astrocytes in the hippocampus.

On the one hand, early-stage research has demonstrated that endogenous SP exerted proinflammatory influences on epithelial and immune cells in inflammatory-related diseases of the musculoskeletal, respiratory and gastrointestinal systems[52]. The release of SP was elevated in the intestine following the stimulation of hrIL-1β or TNBS[53,54]. Colitis was alleviated in $TRPA1^{-/-}$ mice and by TRPA1 pharmacologic inhibitor or NK-1R antagonists[54,55]. As reported in an earlier study on neuropeptide Y[56], we hypothesize that SP's role in mediating inflammatory responses is linked to immune activation under adverse conditions, reflecting the organism's self-regulatory and self-defensive mechanisms. On the other hand, after DSS removal for an additional 5 days, mice exhibited reduced colitis scores and mild body weight loss, whereas mice treated with the NK-1R antagonist during the recovery phase showed increased colitis clinical scores and further decreased body weight[57]. Exogenous SP is found to have anti-inflammatory and antioxidant properties. SP exerted significant effects in protecting against cardiovascular dysfunction, skin injury, intestinal disorders and cholestatic liver injury[58–61]. SP improved wound healing via promoting cell proliferation and migration in vitro and in vivo[62,63]. SP's dual role may depend on multiple factors, including clinicopathological conditions, the stages of disease development, and SP source (endogenous or exogenous). Our study demonstrates the beneficial effects of exogenous SP in colitis.

There has been a growing body of research focusing on the contributions of neurotransmitters, such as 5-HT and GABA, to gut and brain health[64–66]. Neuropeptides are also an important class of neurotransmitters expressed within the CNS and peripheral tissue[26]. Among these neuropeptides, SP has been reported to play a central role, exerting anti-inflammatory and neuroprotective effects that can alleviate ischemic brain injury[67]. Our previous work has found the key role of SP in maintaining intestinal barrier function in DSS-induced colitis[26]. Here, we further demonstrated that SP could ameliorate DSS-induced anxiety-like behavioral disorders, mitigate hippocampal pathological lesions, and suppress the generation of neuroinflammatory factors. Microglia are the primary immune cells in the brain, and when they become activated, they release inflammatory mediators that induce a neuroinflammatory state to disrupt the balance of neurotransmitters, thereby eliciting anxiety-like manifestations linked to IBD[68–70]. In line with these findings, the number of activated microglia in the hippocampus was increased in the DSS group; however, SP treatment reversed this change in microglia count. Building upon the previous study that demonstrated deleterious microglia with M1 phenotype mediate neuroinflammatory responses in various brain diseases[71], we next analyzed whether SP regulated the polarization of activated microglia. As expected, our results demonstrated that the suppression of overactivated inflammatory M1 microglia is one of the possible reasons for SP reducing hippocampal neuroinflammation. Additionally, increasing evidence indicates that astrocytes are implicated in affective and mood disorders. Unexpectedly, GFAP expression was significantly decreased in the hippocampus of the DSS group, which contrasts with previous reports indicating that astrocytes are activated during inflammation[72]. Nonetheless, astrocyte activation in the hippocampus is known to elicit anti-anxiety effects[73,74]. Evidence of reduced GFAP immunoreactivity following traumatic brain injury (TBI) has been documented, attributed to the breakdown of intermediate filaments and accompanying alterations in overall protein function[75]. Given that TBI induces neuroinflammation in the hippocampus, a similar mechanism may underlie the reduced GFAP observed in the hippocampus of the DSS-induced colitis model mice. Consistent with our findings, Zhang et al. demonstrated that GFAP expression was significantly lower in DSS-induced colitis compared to control mice. Interestingly, GFAP level in the hippocampus increased following electroacupuncture or moxibustion treatment[76]. Astrocytes play crucial roles in supporting neurons by facilitating the exchange of metabolic and nutritional materials, maintaining ion concentrations, and clearing neurotransmitters in their vicinity[77]. Dickerson et al. reported decreased level of GFAP in the hippocampus 52 weeks after blast injury[78]. More importantly, animals with lower levels of GFAP and MAP2 exhibited more pronounced anxiety-like behaviors. They suggested that a decrease or dysfunction of astrocytes could disrupt the tripartite synaptic structure between astrocytes and neurons, potentially diminishing neuronal communication and neurotransmitter release, and leading to anxiety-like and depressive behaviors. In our study, the reduction of hippocampal astrocytes in the DSS group may indicate that their neuroprotective function is compromised. Conversely, SP treatment could activate GFAP expression in the hippocampus, thereby improving neurological deficits. Thus, the activation of astrocytes has significant implications for brain protection. Furthermore, the alteration of astrocytes may depend on the timing and context of the disease. Do et al. demonstrated that GFAP alterations varied by brain region and duration of DSS exposure. In the hippocampus, both mRNA and protein expression of GFAP were elevated after 3 days of DSS exposure, but a downregulation was observed by day 7[79]. Similar findings have been noted in depression[74,80]. Based on these results, we propose that early activation of astrocytes during the progression of anxiety-like disorders induced by colitis may lead to subsequent astrocyte dysfunction, warranting further investigation. Consequently, our study suggests that SP suppresses microglial activation in DSS-induced mice. Importantly, we found that SP rescued the

loss of GFAP-labeled astrocytes, contributing to the improvement of neurological deficits in the hippocampus, which may be one of the mechanisms through which SP exerts its anti-anxiety effects. Nonetheless, further research is warranted to elucidate the mechanism by which SP exerts anxiolytic impacts in emotional disorders linked to IBD.

It is now widely accepted that gut microbiota promotes bidirectional communication between the brain and the gastrointestinal tract. Alterations in the composition and activity of the intestinal flora have been correlated with various neurological and psychiatric conditions[81,82]. Neurotransmitters are likely to emerge as neural messengers and affect the activity of the intestinal microbiota to orchestrate the bidirectional gut-brain communication[21]. Ma et al. found that 5-HT mitigates chronic stress-induced cognitive deficits by modulating the intestinal microbiome[83]. Another study investigated GABA and demonstrated that it can enhance intestinal mucosal immunity, which might be related to the altered gut microbiota structure[84]. However, the influence of the neuropeptide SP on the crosstalk between the gut microbiome and the brain awaits to be explored. Therefore, it is still worthwhile studying whether SP influences gut microbiota to ameliorate IBD-like symptoms and mental disorders. Numerous studies have shown that SP has antimicrobial activity and could regulate the virulence of *Bacillus cereus*, *Staphylococcus aureus*, and *Staphylococcus epidermidis*[85]. Prior studies have identified a connection between gut microbiota changes and IBD pathology, specifically, and stabilizing the gut microbiota is able to mitigate IBD-related symptoms and neuroinflammation[86]. Our 16S rRNA gene sequencing data revealed that the dominant microbiota belonged to the *Bacteroidaceae* and *Enterobacteriaceae*, and *Escherichia_Shigella* was the predominant genus-level taxa in mice of the DSS group. In the DSS + SP group, the representative microbiota was *Lachnospiraceae* and *Muribaculaceae* at the family level, and at the genus level, *Prevotellaceae_UCG_001*, *unclassified_Muribaculaceae* and *unclassified_Lachnospiraceae* were identified as dominant microbiota. Several studies have shown that microbiota dysbiosis is characterized by the proliferation of bacteria belonging to the *Enterobacteriaceae*[87], and *Lachnospiraceae* and *Muribaculaceae* are the key family of bacteria to improve intestinal impairment in IBD[88,89]. The abundance of *Enterobacteriaceae* was higher in the fecal samples of patients with both IBD and depression in comparison to those with IBD alone[90]. Administering *Enterobacteriaceae* and *Escherichia coli* individually or in combination via gavage resulted in the development of colitis and depression-like symptoms in germ-free and specific pathogen-free mice[91]. These gram-negative bacteria could affect systemic inflammation and brain function via their by-products, including lipopolysaccharides and exopolysaccharides[90]. Additionally, probiotic bacteria might exert a positive impact on mental health by enhancing mood and sleep quality[92]. To further, our study showed that the beneficial effects of SP on preventing gut and hippocampus from damage are significantly impaired post-ABX intervention, indicating that the gut microbiota that are susceptible to antibiotics could be a crucial factor in SP's mitigation of anxiety-like behaviors. A previous study demonstrated that the transplantation of fecal microbiota from patients with IBD increased the expression of inflammatory genes in the colonic tissues of recipient SPF mice, and also induced anxiety-like behaviors in these mice[93]. By contrast, improving the composition of intestinal microbiota could mitigate depressive and anxiety-like symptoms[94]. Likewise, in our study, 16S rRNA gene sequencing analysis suggested that FMT from mice treated with DSS + SP could ameliorate gut dysbiosis by elevating the relative abundance of g_*unclassified_Muribaculaceae*, g_*unclassified_Lachnospiraceae* and g_*Lactobacillus*, while decreasing the abundance of g_*Bacteroides* and g_*Ligilactobacillus*. As expected, the FMT-DSS group exhibited gross symptoms of colitis and intestinal mucosal injury, along with anxiety-like disorders and hippocampal inflammation, compared to the FMT-CON group. However, recipient mice accepted fecal microbiota from the FMT-DSS + SP group showed significantly improved pathological changes. More importantly, mice receiving gut microbiota from the DSS + SP group exhibited decreased M1-like microglia, but increased M2-like microglia in the hippocampus. Compared with the FMT-DSS group, down-regulated astrocytes were rescued in the FMT-DSS + SP group. These data highlighted that the administration of SP mitigated DSS-induced intestinal dysbiosis, which accounted for the protective effects of SP on gut barrier and mental health. Nonetheless, the effect of microbiota alteration on the emergence of neuropsychiatric disorders requires deeper exploration.

We next investigated the potential mechanisms of SP against anxiety-like behavior via altering intestinal flora. Transcriptome data suggest that the NF-κB pathway is up-regulated in the hippocampus of mice following FMT-DSS treatment compared to FMT-CON mice, however, FMT-DSS + SP treatment inhibited the activation of the NF-κB pathway. It has been well documented that the activated NF-κB signaling pathway in microglia mediates neuroinflammation in various neurological diseases[95]. Our result verified that the *p65* and *IKBα* gene expressions as well as p-p65 and p-IKBα protein levels were lower after FMT-DSS + SP treatment compared to the FMT-DSS group. Particularly, immunofluorescence assay revealed that the p-IKBα-positive signal in microglia was weakened in the FMT-DSS + SP group, compared to the FMT-DSS group. Interestingly, the RNA-sequencing data also revealed the neuroactive ligand-receptor interactions and Ca^{2+} signaling pathways were up-regulated in the hippocampus of the FMT-DSS + SP group compared with the FMT-DSS group. Detailed analysis uncovered a significant increase in the gene expression of $GABA_AR$ and $GABA_BR$ with distinct subunits after FMT-DSS + SP treatment. We further conducted western blot assay to validate the aforementioned data. Results suggested that the expressions of $GABA_AR$, $GABA_BR$, and GAD65 were strongly enhanced in the hippocampus of mice treated with FMT-DSS + SP than in mice treated with FMT-DSS. There is increasing support that a marked deficit in GABAergic synaptic transmission has been observed in anxiety disorders and major depression[96,97]. More recently, modulators of α2α3 $GABA_A$ receptor subtypes and $GABA_BR$ agonists have found initial clinical proof in the therapy of anxiety disorders[97,98]. Therefore, the increased expression of key molecules implicated in the GABAergic neurotransmission pathway may explain the amelioration of anxiety-like behaviors in mice treated with FMT-DSS + SP. It has been found that ionotropic $GABA_AR$ activation evokes membrane depolarization and could elevate the calcium concentration $[Ca^{2+}]i$, thereby modulating a variety of $[Ca^{2+}]i$-dependent cellular processes[99–101]. The metabotropic $GABA_BR$ activation enhances the $[Ca^{2+}]i$ elevation triggered by the metabotropic glutamate receptor mGluR1[102,103]. $GABA_A$ and $GABA_B$ receptors interact to elicit a full Ca^{2+} response in cerebrovascular endothelial cells[42], and they synergistically elevate intracellular Ca^{2+} in mouse embryonic stem cells[104]. In our study, the RNA-seq results revealed similar trends, indicating that the FMT-DSS + SP treatment also could promote downstream Ca^{2+} signaling in the hippocampus, as evidenced by increases in a series of genes involved in the process of Ca^{2+} signaling. In addition, as a sensitive sensor of Ca^{2+} concentration, calmodulin (CaM) specifically binds with Ca^{2+}, and then the CaM-Ca^{2+} complex can interact with target CaMKII[105,106]. Consistently, our study suggested that the administration of FMT-DSS + SP significantly elevated the CaMKII expression in the hippocampus. Although previous studies reported that astrocytes might be implicated in the process of psychiatric disorder, the putative mechanisms by which astrocytes impact affective state require further to be elucidated[107]. In this regard, Cho et al. proposed unexpected evidence that intracellular Ca^{2+} activation of hippocampal astrocytes induced anxiolytic behavior, which was dependent on modulating ATP-mediated synaptic homeostasis[73]. Based on the transcriptomics data and the demonstrated ability of SP to prevent astrocytes loss, we speculated that SP might exhibit anti-anxiety activity by modulating relevant signaling pathways in

astrocytes. To verify this conjecture, we found that $GABA_AR\alpha1$-positive expression in astrocytes of the hippocampus was significantly higher in the FMT-DSS + SP group than in the FMT-DSS group. Likewise, the administration of FMT from the SP-treated group increased the signal of CaMKII-positive in the astrocytes of the hippocampus but not FMT from the DSS-treated group. To further, RNA sequencing of flow-sorted microglia and astrocytes elucidated that FMT-DSS + SP dampened NF-κB activation in microglia while enhancing the GABAergic and subsequent Ca^{2+} signaling in astrocytes. Overall, the combination of fecal microbiota transplantation experiments and RNA sequencing demonstrates that gut microbiota's putative effects were critical in the process of SP against colitis and anxiety-like behavior, which is associated with the inhibition of NF-κB in microglia and activation of the GABAergic/Ca^{2+} signaling in astrocytes.

Gut microbiota-derived metabolites have been suggested to serve as signaling molecules that potentially cross the blood-brain barrier and facilitate the gut-brain axis to affect neurophysiology and behavior[108]. Gut microbiota has the capability to both synthesize and metabolize a diverse array of classical neurotransmitters, including dopamine, serotonin, and γ-aminobutyric acid[109]. In our study, metabolomics analysis showed that intervention of SP caused an increase in the content of GABA and dopamine, which exhibited the ability to reduce anxiety symptoms[110,111]. Notably, inositol was significantly enriched after the SP intervention. Recent studies have established inositol triphosphate, produced by intestinal flora metabolizing dietary phytic acid, induces HDAC3 activation, ultimately encouraging intestinal epithelial cell proliferation as well as intestinal barrier repair in inflammatory bowel disease[112]. Importantly, intestinal flora can synthesize inositol phosphate, which is involved in neuronal signaling and osmoregulation[113,114]. In the present study, inositol was orally administered to DSS-induced colitis mice to further verify the beneficial effects of inositol. As expected, the administration of inositol was demonstrated to protect against colitis. In terms of the regulation of mental dysfunction, inositol significantly mitigated behavioral disorders through alleviating hippocampal damage and neuroinflammation. Moreover, after inositol treatment, there was a reduction in the number of microglia. We speculated that inositol may target microglia to dampen the neuroinflammatory response in the hippocampus. Nevertheless, it was not clear how inositol affects IBD-related psychiatric disorders needs to be further explored. Here, a preliminary study was conducted, and results showed that the supplement of inositol promoted the synthesis of GABA in the hippocampus, and the expression of $GABA_AR$ and $GABA_BR$ was significantly increased by the inositol supplement. In fact, the activity of GABA at the synaptic cleft is terminated through reuptake into nerve terminals and astrocytes, mediated by membrane-located GATs, and GAT-facilitated reuptake processes therefore play a key role in shaping GABAergic neurotransmission[115]. Surprisingly, inositol supplement could increase the number of astrocytes, and especially, GAT1-immunopositive expression was evidently up-regulated. To investigate the role of inositol in the neuroprotective effects of SP, mice were treated with the inositol synthesis inhibitor, L-690330. Results indicated that L-690330 reversed the anxiolytic effects of SP and the improvements in hippocampal damage. Further analysis revealed significant increases in inositol concentration in both the hippocampus and serum following treatment with FMT-DSS + SP. We speculated that inositol may have a direct impact on the hippocampus. In vitro assay supported this hypothesis, demonstrating that inositol improved LPS-induced neuroinflammatory responses in BV-2 cells, and attenuated the downregulation of the GABAergic /Ca^{2+} signaling pathway induced by LPS in C8D1A cells. These findings suggest that inositol, as a key metabolite of the microbiome-gut-brain axis, mediates the effects of SP on the improvement of intestinal impairment and anxiety-like behaviors in DSS-induced mice. Multi-omics combined analysis explored the relationship among host phenotypes, gut microbiota, metabolites, and brain gene transcription. The results showed that SP improved gut dysbiosis and further increased microbial-derived inositol, which influenced the transcription of hippocampal genes related to the NF-κB, GABAergic neurotransmission, and Ca^{2+} signaling pathway. These changes contributed to the amelioration of DSS-induced intestinal lesions and anxiety-like behaviors. Previous studies in TNBS-induced colitis models have reported the presence of aberrant behaviors in anxiety-like and depressive-like tests[116]. Finally, we demonstrated that SP could alleviate TNBS-induced colitis and improve hippocampal damage and anxiety-like behaviors.

There are some limitations within our study. Firstly, although we conducted anxiety-like behavioral tests without colonic inflammation following DSS withdrawal, innovative behavioral assays need to be developed to directly obtain anxiety-like behavioral results without confounding factors, including locomotor activity. Secondly, no obvious signs of toxicity or adverse side effects were observed in the experiments conducted, indicating that SP exhibits promising potential to be developed into an effective therapeutic agent. Nevertheless, further studies will be warranted to conclusively evaluate the efficacy and long-term safety of SP in patients with ulcerative colitis. Thirdly, the emerging role of gut microbiota in improving TNBS-induced colitis has recently been highlighted[116]. Upcoming research will continue to explore the precise mechanisms by which SP exerts its protective effects in TNBS-induced animal models of Crohn's disease. Finally, we believe that an adoptive transfer of microbiota experiment is necessary to obtain direct evidence for a comprehensive understanding of the role of gut microbiota in SP's effects on colitis and anxiety-like behavior in future research.

Collectively, our results suggest that SP effectively ameliorated IBD-like gastrointestinal impairment and psychiatric disorders via the microbiota-gut-brain axis, which was achieved by restoring microbial dysbiosis and subsequently augmenting the production of the microbiota-derived metabolite, inositol. Through the putative role of intestinal microbiota, as well as inositol, SP inhibited the NF-κB pathway in microglia, and activated GABAergic neurotransmission and downstream Ca^{2+} signaling within astrocytes in the hippocampus, thereby contributing to the reduction of neuroinflammation and improvement of anxiety-like behavior. Our work reveals a crucial, previously undiscovered role for SP in modulating the microbiota-gut-brain axis, highlighting SP as a promising therapeutic candidate for diseases where gastrointestinal and anxiety-related symptoms are interconnected (Fig. 10).

Methods

Study procedure

A flowchart of the experimental design in this study is shown in Supplementary Fig. 1.

Animals

All animal experiments have been approved by the Institutional Animal Care and Use Committee of China Agricultural University (AW92303202-2-1, A0090214202-2-02). 7- to 8-week-old specific pathogen-free (SPF) male C57BL/6J mice (Vital River Laboratory Animal Technology, Beijing, China) were housed under a standard SPF facility in an environment (23–25 °C, 45–55% humidity and 12-h light/12-h dark cycle). All mice were adapted to the environment and allowed to receive a standard diet and water for one week. At the end of the experiment, mice were euthanized humanely by CO_2 asphyxiation followed by cervical dislocation. All procedures adhered to the principle of minimizing distress.

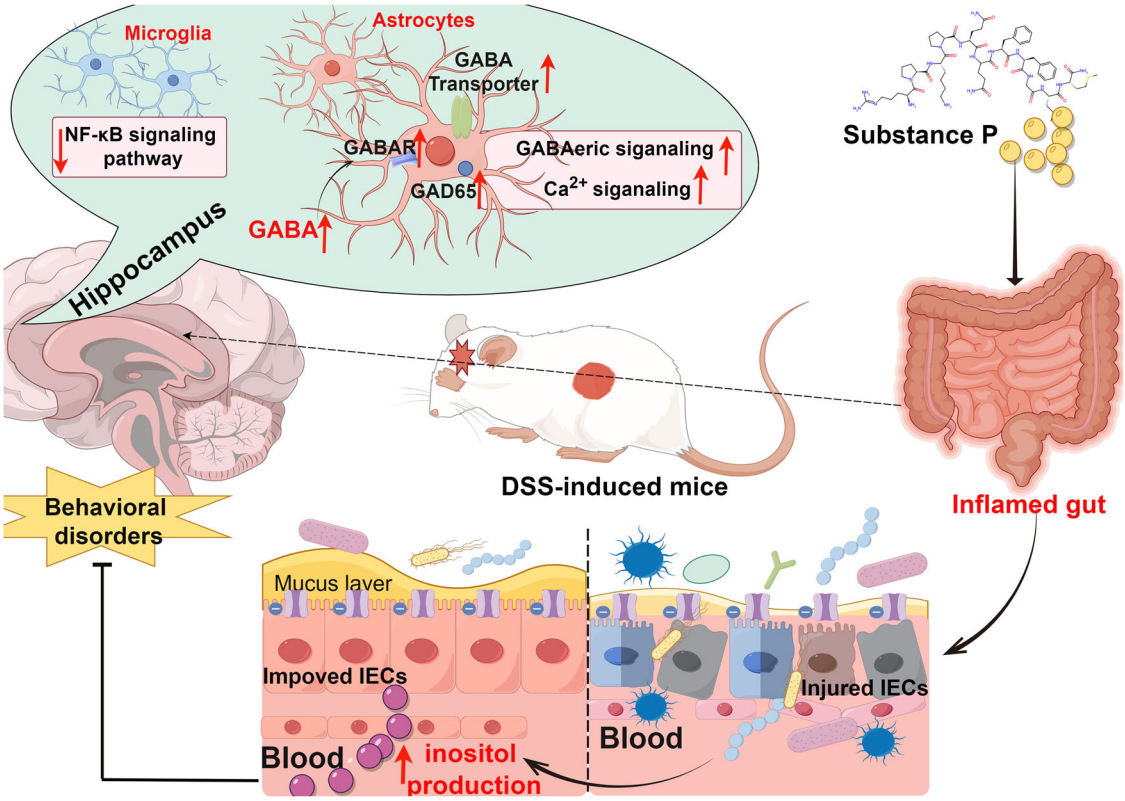

Fig. 10 | The schematic diagram explains the mechanism underlying by which SP protects against colitis and anxiety-like behavior. Administration of SP effectively mitigated DSS-induced intestinal impairment and behavioral disorders by improving microbial dysbiosis and subsequently promoting the enrichment of the microbiota-derived metabolite, inositol. Furthermore, the antianxiety activity of SP involves suppressing NF-κB pathway while activating GABAergic neurotransmission and downstream Ca^{2+} signaling in the hippocampus. We painted mechanism schemes by figdraw.com.

Dextran sodium sulfate (DSS)-induced colitis and experimental design

Acute colitis was induced by administering 4% DSS (molecular weight 36–50 kDa; Yeasen, Shanghai, China) dissolved in drinking water for 6 days. Mice were monitored daily for body weight and assessed for the disease activity index (DAI). According to previous reports, DAI is considered a standard measurement of UC severity and prognosis, which comprises three indicators: weight loss (scored from 0 to 4 based on a loss of 0 to 15%), stool consistency (0 points for normal, 2 points for loose stool, and 4 points for diarrhea) and hematochezia (0 points for normal, 2 points for positive occult blood, and 4 points for overt hemorrhage)[117].

Study 1: treatment with SP

The experimental design is shown in Fig. 1a. The mice were randomly divided into four groups (ten mice in each group) as follows: normal control (CON), DSS only, DSS + SP (5 nmol/kg), and SP (5 nmol/kg) alone. The DSS group was provided free access to 4% DSS, and injected with sterile saline daily for 6 days. The DSS + SP groups received 4% DSS for 6 days, and SP (5 nmol/kg/day in sterile saline) was administrated by injection. The SP alone group was given normal water and SP (5 nmol/kg/day in sterile saline) for 6 days. All mice underwent a series of behavioral tests. The feces status and weight changes were daily recorded. Furthermore, the hippocampal tissues and colon tissues, colonic contents, and fecal samples were collected were harvested for additional analysis.

Study 2: antibiotic treatment

To explore the potential role of gut microbiota in mitigating DSS-induced colitis through SP, a comprehensive experimental design was employed. Initially, all mice underwent a 14-day ABX treatment of a mixture of antibiotics (Meilune, Dalian, China) including 1 g/L ampicillin, 1 g/L metronidazole, 0.5 g/L vancomycin, 0.5 g/L neomycin and 0.1 g/L gentamycin in drinking water to effectively deplete the gut microbiome[118]. The antibiotics were changed every other day. After 2 weeks of ABX treatment, mice were randomly assigned to three groups: ABX (CON), ABX (DSS), and ABX (DSS + SP) groups. The SP treatment and DSS-induced colitis remained consistent with Study 1 of this study. The samples collected were consistent with those collected in the above study. All mice were euthanized on day 20 following the protocol outlined in Fig. 4a.

Study 3: fecal microbiota transplantation (FMT)

To further validate the ameliorating effect of SP on DSS-induced colitis in a gut microbiota-dependent manner, we performed an FMT experiment following the protocol established in a previous study[119]. Initially, we collected the feces of CON, DSS, and DSS + SP groups according to Study 1 as the donors of FMT. Collected fresh feces samples were quickly conserved in 40% sterile glycerol under −80 °C. Before FMT, for substantial depletion of the microbiota, recipient mice have undergone a 2-week ABX treatment as outlined in Study 2 of the protocol. Subsequently, the mice were randomized into three groups: FMT-CON, FMT-DSS, and FMT-DSS + SP groups. Each sample of 100 mg feces was suspended in 1 mL of sterile phosphate-buffered saline (PBS) and centrifuged at 800 × *g* for 5 min to separate the supernatant. The bacterial suspension was filtered twice and then gavaged to the recipient mice (150 µl per mouse) for 7 d. Afterward, the mice in the FMT-DSS and FMT-DSS + SP groups were treated with 4% DSS. The samples collected were consistent with those collected in the above study. The experimental timeline is shown in Fig. 5a.

Study 4: inositol intervention

To investigate the protective effects of inositol on anxious behavior in colitis mice, mice were assigned to four groups. For the control group

(CON), mice received normal water for 14 days throughout the study. For the group treated with DSS (DSS), mice received normal water for 8 days, and then 4% DSS was administrated in their drinking water for 6 days. For the group treated with inositol and DSS (DSS+inositol), mice were treated with 2% (w/v) inositol (CAT#87-89-8; MACKLIN, China) in the drinking water for 8 days prior to 4% DSS administration and continued to receive treatment for 6 days during DSS treatment. For the group treated with inositol alone, mice received drinking water with 2% (w/v) inositol for 14 days. Behavioral tests were performed on the last day. The samples collected were consistent with those collected in the above study. The experimental procedure is comprehensively illustrated in Fig. 8a.

Study 5: administration of inositol synthesis inhibitor

To investigate the role of inositol in the action of SP against anxious-like behaviors in DSS-induced mice. The mice were divided into three groups: (1) DSS group, (2) DSS + SP group, and (3) DSS + SP + L-690330 (inositol synthesis inhibitor) group. DSS and SP administration design was the same as in Study 1. L-690330 was diluted in saline and injected intraperitoneally administered at a dose of 0.1 µmol 1 h prior to SP injection. Saline was treated as a vehicle control. The experimental design is shown in Fig. 9a.

Hematoxylin and Eosin (H&E) staining

The fresh colon and brain tissues were randomly sampled from each experimental group and subsequently fixed with a 4% paraformaldehyde solution for a duration of 48 h. Following the fixation step, the tissues were dehydrated through a graded series of ethanol solutions, then cleared with xylene, and finally embedded in paraffin. The paraffin-embedded samples were sectioned into 6 µm-thick slices. These sections were then subjected to a routine deparaffinization process. Following this, tissue sections were stained with hematoxylin and eosin (Beijing Solarbio Science & Technology Co., Ltd.). Then, the sections were rapidly differentiated, and dehydrated using 95% ethanol. The samples were then cleared with xylene and finally sealed using a neutral gum sealant. After H&E staining, colon crypt depth was assessed using ImageJ software (version 2.14.0). Histological scores were evaluated by an investigator blinded to the experimental groups according to inflammatory infiltration, mucosal damage, and destruction of the intestinal epithelium, as previously reported in Table S2[120,121]. For H&E staining of brain tissue, the tissue morphology of the hippocampal DG, CA1, and CA3 regions was examined under a light microscope. Image Pro Plus 6.0 software was used to quantify the number of cells with lesions in the hippocampal DG, CA1, and CA3 regions.

Transmission electron microscope

To visualize the ultrastructure of tissue, colonic segments were cut into 1 mm^3 samples and fixed in 2.5% glutaraldehyde and 1% osmium tetroxide at 4 °C overnight. Then, the samples were dehydrated in ethanol and embedded in epoxy resin, and finally were sliced into ultrathin sections. The slices were stained with uranyl acetate and lead citrate, and observed under a TEM-1400 Plus electron microscope (JEOL JEM-1400 Plus, Tokyo, Japan). Representative images illustrating tight junction structures and microvilli were chosen.

Alcian Blue-Periodic Acid-Schiff (AB-PAS) staining

The 6-µm-thick colon slices obtained by the above method also were stained with an AB-PAS kit (Solarbio, G1285, Beijing Solarbio Science & Technology Co., Ltd., Beijing, China) following the instructions. After dewaxing and hydration, the slides were incubated in AB for 20 min and then were washed with water, followed by incubation in 1% periodic acid for 10 min. After the appellate step, the slides were incubated in Schiff's reagent for 10 min. The slides were finally re-stained with hematoxylin for 30 s, washed and dehydrated, and then fixed with Pertex. The stained sections were observed under an optical microscope (Leica). The number of goblet cells per crypt was counted based on the typical morphological structure using Image Pro Plus 6.0 software.

Immunofluorescence staining

Briefly, after deparaffinization, rehydration, and antigen retrieval, slides were blocked with donkey serum for 30 min at room temperature following incubation with primary antibodies against GFAP (1:1000, A8335, 1:200, NB100-53809, USA), Iba-1 (DF6442, 1:200, Affinity, China), E-cadherin (PB9561, 1:200, Boster, China), Mucin 2 (bsm-60016R, 1:100, Bioss, China), $GABA_AR\alpha1$ (1:200, 12708-1-AP, Proteintech, China), calcium/calmodulin-dependent protein kinase II (CaMKII) (1:50, ab76703, Abcam, UK) and p-IKBα (1:100, WLH3930, Wanleibio, China) at 4 C overnight. Then, slides were washed three times in PBS and incubated with biotinylated secondary antibodies (705-065-147, Jackson, USA) at 4 °C overnight. After incubation with the fluorescent antibody at 37 °C for 2 h slides were washed three times in PBS, dried, and treated with 4′,6-diamidino-2-phenylindole (DAPI) (0100-20, SouthernBiotech, Birmingham, AL, USA). The images were collected under a confocal laser-scanning microscope (Nikon, Tokyo, Japan). Additionally, image Pro Plus software was used to calculate positive cell count and average fluorescence intensity in the hippocampal DG, CA1 and CA3 region.

Intestinal permeability assay

Intestinal permeability was evaluated by using fluorescein isothiocyanate-conjugated dextran (FITC-dextran, molecular weight: 4 kD). Briefly, all mice were fasted for 6 h, and then FITC-dextran solution (Chondrex, Redmond, WA, USA) at the dose of 20 mL/kg was delivered via oral gavage. After 4 h, blood samples from the eyeballs were collected and the fluorescence intensity in serum was determined on a fluorescence spectrophotometer (excitation, 485 nm; emission, 528 nm).

The Luminex multiplex bead array

The Luminex analysis was conducted by LabEx (Shanghai, China). Utilizing the Bio-Plex Pro Mouse Cytokines Grp I Panel 23-plex kit, the expression levels of 23 cytokines were quantified, adhering strictly to the manufacturer's instructions. In brief, homogenates from mouse colon and hippocampus tissues were gathered and incubated in 96-well plates along with diluent microbeads for half an hour in a darkened setting at ambient temperature. Following the removal of supernatants, the samples underwent exposure to detection antibodies for an additional 30 min in a room-temperature environment. Afterward, Streptavidin-PE was introduced to each well and allowed to incubate for 10 min at room temperature.

Open-field test (OFT)

The OFT was conducted to assess exploratory activity and spontaneous locomotor function in mice[122]. Behavioral experiments were conducted in an enclosed, opaque chamber with a square layout by the open-field equipment. Mice were gently deposited in the central zone of a white table platform, with the testing conducted under conditions of low lighting and minimal ambient noise. All mice underwent an acclimatization to the environment for 5 min and moved freely, during which the total moving distance of mice, the time spent in the central region, distance of the central region, as well as moving speed in the central region.

Elevated plus-maze (EPM)

EPM is commonly used in rodents to assess exploratory and locomotor activity, unconditioned fear, and potential anxiety[116]. The elevated plus-maze (EPM) consists of open arms and closed arms that extend

perpendicularly from a central platform, which measures 35 cm in length and 5 cm in width, with the closed arms standing 20 cm high. The maze was positioned 60 cm above the ground in a quiet room. Each mouse was placed at the center of the plus-maze, facing one of the closed arms. During a 5-min observation period, the movement distance, number of entries, and duration spent in the open arms were recorded.

Light-dark box (LDB)

In the LDB test, the light-dark box consisted of the light chamber (27 × 30 cm) with a bright light in the center, whereas the dark chamber (27 × 30 cm) had black walls and no light source. The two chambers were interconnected by a rectangular passage measuring 15 cm. The mouse was initially placed in the bright chamber, facing away from the opening, and was given the freedom to explore the entire box. Each mouse's behavior, including the frequency of entries into each area and the time spent in the light box or the dark box, was recorded during a 5-min session.

Elevated zero maze (EZM)

We used the EZM test because of its established predictive validity. Maze has four quadrants (two open zones with 1.5 cm high translucent edges that were separated by two closed zones with 20 cm high walls; platform width was 6 cm wide). Briefly, mice were put in the maze and recorded for 5 min, then immediately removed from the maze. Time spent and distance traveled in the closed and opened zones, as well as the number of entries into each quadrant were interpreted as a reduction of anxiety-like behavior.

Nissl staining

The brain tissue was fixed with 4% polyformaldehyde solution, dehydrated with gradient ethanol, cleared with xylene, embedded in paraffin, and sliced continuously at 6 μm. The sections were stained at 56 °C for 50 min using Nissl reagents (Wuhan Servicebio Technology Co., Ltd.), complying with the manufacturer's guidelines. Next, they were dehydrated with gradient alcohol and transparent with xylene. Finally, the slices were fixed with neutral resin. In the hippocampal tissue of each group, Nissl bodies and pathological changes in neurons were carefully examined under an optical microscope. Slices were randomly selected for each group to count the number of positive neurons (Nissl+ cell) by Image Pro Plus 6.0 software.

Western blotting

The brain and colon tissues were collected after the mice were sacrificed. Proteins were isolated and quantified by a protein assay kit (Beyotime Biotechnology, Shanghai, China), followed by electrophoretic separation. Afterward, the protein was transferred to polyvinylidene difluoride (PVDF) membranes, and then the membranes were blocked in 5% skim milk for 2 h at 37 °C. Next, primary antibody against GFAP (1:1000, A8335, 1:200, NB100-53809, USA), $GABA_AR\alpha1$ (1:1000, 12708-1-AP, Proteintech, China), $GABA_BR2$ (1:1000, 27567-1-AP, Proteintech, China), CaMKII (1:1000, 12716, Cell Signaling Technology, USA), GAD65 (1:1000, ab239372, Abcam, USA), CD206 (1:1000, ab64693, Abcam, USA), iNOS (1:1000, 18985-1-AP, Proteintech, China), CD80 (1:1000, 66406-1, Proteintech, China), p-p65 (1:1000, A00284-1, Boster, China), p-IKBα (1:1000, WLH3930, Wanleibio, China), and β-actin (50201, 1:1000, Kemei Borui Science and Technology, China) were incubated with the membranes overnight at 4 °C. After incubation with goat-anti-rabbit IgG secondary antibody (115-035-071, Beyotime Biotechnology, Shanghai, China) for 1 h at 37 °C. The ECL chemiluminescence kit (Tanon Science and Technology Co., Ltd) was used to visualize protein bands, and were observed by a luminometer (Tanon® 5200Multi). β-actin was used as an internal control. ImageJ software (version 2.14.0) was used for analysis of Western blots.

Feces culture and colony-forming unit (CFU) measurement

Feces were collected in a sterile tube and diluted with 10-weight volume of PBS. The tube was vigorously vortexed. Then, the samples were centrifuged at 100 × *g* for 10 min. The supernatant was serially diluted to 10^2 to 10^8 folds and then was streaked with a cell spreader on an LB agar plate. After incubation at 37 °C for 24 h, CFUs were measured.

Fecal DNA extraction and quantification

After the experiment, fecal samples were collected to assess fecal DNA content. DNA was extracted from fecal samples (100 mg) of mice, using the QIAamp DNA Stool Mini Kit (Qiagen, Hilden, Germany) based on the manufacturer's instructions. The DNA purity and concentration were measured with a NanoDrop 2000C spectrophotometer (Thermo Scientific).

16S rRNA sequencing analysis

Microbiome bioinformatic analysis was performed by the Biomarker Technologies Co., Ltd (Beijing, China). Briefly, total microbial DNA was extracted from colonic contents. The V3-V4 region of the 16S rRNA gene is amplified from the extracted DNA using universal bacterial primers that target conserved regions of the gene. PCR products were quantified by the Quant-iT PicoGreen dsDNA Assay Kit. The 16S rRNA gene amplicons are then prepared for high-throughput sequencing using the Illumina Novaseq platform (Biomarker Technologies, Beijing, China). The raw reads from sequencing were filtered using Trimmomatic v0.33 and cutadapt 1.9.1 to obtain high-quality clean reads. Afterwards, chimera sequences were detected and then removed using the DADA2 Algorithm[123]. Finally, the qualified sequences were clustered at a 97% similarity level using USEARCH (version 10.0), and 0.005% of the total sequences were identified as quality-filtered sequences to generate the amplicon sequence variants (ASVs). Taxonomy was assigned to the ASVs using the classify-sklearn at a 70% confidence threshold. The representative sequence for each ASV was screened for further annotation. Alpha diversity indices, including the Chao1, Shannon, and Simpson indices, were calculated using QIIME2 software (Version 2020.8)[124]. Statistical significance between groups was determined by one-way analysis of variance (ANOVA) using BH-FDR methods based on python2 software (scipy v0.17.1). Beta diversity analysis was performed to investigate the structural variation in microbial communities across samples using binary Jaccard distance metrics and visualized via principal coordinates analysis (PCoA). Permutational multivariate analysis of variance (PERMANOVA) based on the binary Jaccard distance was applied to identify statistical significance of beta diversity between groups by using the vegan package in R. The random forest analysis was performed by R v3.1.1 software (randomForest v4.6-10). PICRUSt2 software[125] by referring to the Kyoto Encyclopedia of Genes and Genomes (KEGG) database[126].

Quantitative real-time polymerase chain reaction (qRT-PCR)

Colonic and hippocampal total RNA was isolated using TRI Reagent following the manufacturer's guidelines and then was reverse transcribed using HiFiScript cDNA synthesis kit from Vazyme (Jiangsu, China). The qPCR was carried out on StepOnePlus Real-Time PCR System (Bio-Rad, INC, USA) using SYBR green dye (CWBIO, Beijing, China) following the standard program[26]. The gene expression was normalized to β-actin using the $2^{-\Delta\Delta CT}$ method. The primers were synthesized by Sangon Biotech and sequences of oligonucleotides are shown in Table S1.

Biochemical analysis

Colon tissues were homogenized in PBS and then centrifuged at 16,000 × *g* for 15 min to collect supernatant, which was measured the protein content by a BCA protein assay kit. The concentrations of cytokines was detected using IL-6 (H002-1-1) and TNF-α (H052-1-1)

Enzyme-linked immunosorbent assays (ELISA) kits (Jiancheng Bioengineering Institute, Nanjing, China) in colon tissue. The concentration of SP was detected by an ELISA kit (Elabscience Biotechnology Co., Ltd., Wuhan, China) in hippocampal tissues. The level of MPO of colonic samples was determined using a commercially available kit (H508-1-1, Jiancheng Bioengineering Institute, Nanjing, China). The cytokines γ-Aminobutyric acid (GABA) from the hippocampus samples in each group of mice were assessed using ELISA kits (H168-1-2, NJJCBIO, Nanjing, China). All assays were in accordance with the manufacturer's protocols. A microplate reader (Bio-Rad, Germany) was engaged to obtain optical density (OD) values. The results were calculated in reference to the standard curve.

Transcriptome sequencing and bioinformatics analysis

The samples are derived from the hippocampus tissue of mice as well as two types of cells sorted using flow cytometry. Transcriptome sequencing and data analysis were performed by OE Biotech Co. Ltd (Shanghai, China). Total RNA was extracted using TRIZOL reagent (Invitrogen, USA), including an additional DNase I digestion step. The concentration of the extracted RNA was measured using a NanoDrop ND-2000 Spectrophotometer (Thermo Scientific, Wilmington, USA). RNA quality was evaluated to ensure RNA integrity, as assessed by the Agilent 2100 Bioanalyzer (Agilent Technologies, Santa Clara, CA, USA). RNA-seq libraries were constructed using TruSeq™ RNA Sample Preparation kits (Illumina, San Diego, CA, USA). Bioanalyzer 2100 (Agilent, Santa Clara, CA, USA) was used for quality control and then libraries were sequenced by a NovaSeq 6000 platform (Illumina, San Diego, CA, USA). Following sequencing, raw reads in FASTQ format were processed using fastp software, which eliminated low-quality reads to yield clean reads. Spliced transcripts alignment to a reference (HISAT2) software was used for sequence alignment on the clean reads from each sample. Differential expression analysis was conducted with the DESeq2 (2012) R package[127]. Hierarchical clustering of differentially expressed genes (DEGs) was carried out to illustrate the expression patterns across different groups and samples. KEGG pathway enrichment analyses of the DEGs were performed separately using R, based on the hypergeometric distribution.

UALCAN database analysis

UALCAN (https://ualcan.path.uab.edu/) is open data of the cancer transcriptome[128]. UALCAN was used to estimate the mRNA expression of genes implicated in the NF-κB pathway and GABAergic/Ca^{2+} signaling in colon adenocarcinoma (COAD).

Cell sorting and flow cytometry analysis

Single-cell suspensions were prepared from the hippocampal tissue through enzymatic digestio and resuspended in 40% Percoll and centrifuged at 800 × *g* for 20 min at 15 °C. The supernatant, which contained the myelin, was discarded, and the pellet was then resuspended in cold MACS buffer. Myelin Removal Beads II (130-96-733, Miltenyi Biotec) were utilized according to the manufacturer's protocol.

The cell pellets were treated with Fc receptor blocker to block nonspecific binding in the dark for 15 min at 4 °C. Then the cells were applied to a magnetic-activated cell sorting (MACS) system using Anti-ACSA2 and Anti-CD11b magnetic microbeads (Miltenyi Biotec, #130-097-679 and #130-093-634), according to the manufacturer's instructions. After incubation, the cells were washed with PBS and the cells were resuspended in PB buffer. The cell suspension was applied to the LS column which was placed in the magnetic field of the MACS separator (Miltenyi Biotec). Then, the magnetically labeled cells were flushed into a tube using 5 mL of PBS. Collect the separated target cells and resuspend them in an appropriate FACS buffer.

MACS-pre-sorting cells were reacted with fluorescent-conjugated specific antibodies for 30 min on ice in the dark, washed, and resuspended in FACS buffer. The following antibodies were used for immunofluorescence staining: APC-Cy7-labeled CD45 (103114, Biolegend), PE-labeled CD11b (101208, Biolegend), APC-labeled ACSA2 (130117386, Miltenyi Biotec). The unbound antibody was removed by washing with PBS and centrifuged at 400 × *g* for 10 min. The stained cells were analyzed using BDAriaIII (BD Biosciences) and BD FACS Diva v8.0.1 software.

Ultrahigh performance liquid chromatography-mass spectrometry (UPLC-MS) analysis

Ultrahigh-performance liquid chromatography coupled with mass spectrometry analysis was conducted by Biomarker Technologies Co., Ltd (Beijing, China). Briefly, samples of colonic content and right brain hemispheres (100 mg, ±1%) were weighed and dissolved in 100 µL of acetonitrile/water (1:1, v/v), adequately vortexed, and then centrifuged (13,400 × *g*, 4 °C, 15 min). The supernatants were collected and separated using a UPLC system (1290 Infinity LC, Agilent Technologies). The positive (+) and negative (−) ionization modes of the analytes eluted from the column were detected by electrospray ionization. Analyses were performed using UPLC coupled with quadrupole time-of-flight mass spectrometry (AB SCIEX TripleTOF 6600). During the experiment, quality control samples were utilized to evaluate system stability and data reliability. The original data collected by MassLynx V4.2 were used for peak extraction, peak alignment, and other data processing operations by Progenesis QI software. Based on the Progenesis QI software, online databases such as METLIN[129] and self-built databases of BMG were used for metabolite identification according to sample types. The differential metabolites were identified by combining the *P* value of the t-test and the VIP value of the OPLS-DA model (FC > 1, *P* value < 0.05 and VIP > 1). Differential metabolites were annotated and subjected to enrichment analysis using the KEGG database. Principal components analysis (PCA) and clustering heat maps were performed at MetaboAnalystR[130].

Measurement of inositol level

The levels of inositol in serum and hippocampal tissues were measured using an ELISA kit (Hengyuan Biotechnology Co., Ltd, Shanghai, China), based on the manual of the producer. Hippocampal tissues were blended with PBS (9:1) to homogenate, and then the supernatants were collected by centrifugation at 16,000 × *g* for 15 min. Total protein was analyzed with a bicinchoninic acid method (BCA) protein determination kit according to the manufacturer's instructions.

Immunohistochemical staining

The brain samples were embedded in paraffin wax and then sectioned into 6-µm-thick coronal slices using an automated microtome. The brain tissue sections were carefully spread and baked. Subsequently, the sections underwent a dewaxing process using xylene, followed by rehydration. After rinsing with PBS, the endogenous peroxidases present in the tissue were blocked by treatment with 3% H_2O_2. The sections were blocked with donkey serum and then were incubated overnight at 4 °C with anti-Iba1 antibody (1:200, DF6442, Affinity, China). After PBS washing, the biotinylated secondary antibodies (711-065-152, Jackson, USA) were added to incubate for 2 h at room temperature. Then the slides were washed in PBS and incubated with the VECTASTAIN® ABC Reagent (ZD0201, Vector Laboratories, USA). After washing with PBS, the nuclei were stained using 3,3′-diamino-benzidine-tetrahydrochloride (DAB). Results are expressed as the mean average optical density (AOD) of Iba1-positive and GFAP-positive cells.

Cell culture and treatment

The mouse microglial cell line (BV-2) was purchased from the Chinese Academy of Sciences Cell Bank in Shanghai. BV-2 cells were cultured in Dulbecco's Modified Eagle Medium supplemented with

10% fetal bovine serum (FBS, Gibco), and 1% penicillin-streptomycin in a humidified atmosphere at 37 °C with 5% CO_2. To mimic a neuroinflammatory cellular state, the cells were incubated with LPS at a dose of 1 μg/mL for 24 h. To determine the optimal dosage of inositol, BV-2 cells were pretreated with varying concentrations of inositol (25, 50, and 100 μM) for 2 h. Following this, the cells were continuously incubated with LPS (1 μg/mL) for up to 24 h. The cells were subsequently collected for further analysis.

The mouse neuronal astrocyte cell line (C8D1A) was purchased from Fuheng Biotechnology Co., Ltd (FH0837, Shanghai, China). C8D1A cells were cultured in Dulbecco's Modified Eagle Medium supplemented with 10% fetal bovine serum (FBS, Gibco), 1% penicillin-streptomycin in a humidified atmosphere in a humidified incubator with 5% CO2 at 37 °C. After reaching confluency, C8D1A cells were seeded for desired experiments. Subsequently, to study the action of inositol on astrocyte survival and GABAergic and Ca^{2+} signaling pathway, C8D1A cells were incubated with various concentrations of inositol (50, 100, 200 μM) with or without 1 μg/ml LPS for 24 h. Subsequently, the cells were carefully collected for further assay.

Cell viability was determined by cell counting kit-8 (CCK-8)

Cell viability was evaluated by Cell Counting Kit-8 according to the manufacturer's instructions (MedChemExpress, USA). Cells (1×10^5 cells/ml) growing at the exponential phase were seeded into 96-well plates. BV-2 cells and C8D1A cells were treated with varying concentrations of inositol for 24 h, and the culture medium as control. At the end of treatment, 10 μL CCK8 reagent was added to each well, and incubated with cells for 4 h. Finally, the OD values were detected at 450 nm using a microplate reader. Cell viability was expressed as a percentage of the number of surviving cells relative to the control groups.

Induction of trinitrobenzene sulfonic acid (TNBS) model of mice colitis and SP treatment

The experimental design has been revealed in Supplementary Fig. 23a. Acute UC model of mice was induced using the administration of 2,4,6-Trinitrobenzenesulfonic acid (TNBS) according to the method previously reported[131]. Briefly, mice were lightly anesthetized with ether. Then, 3.5 mg of TNBS (Meilune, Dalian, China) in 100 μL of a 50% ethanol solution was slowly administered into the colon, 3.0–3.5 cm, from the anus, through a flexible catheter. Mice were held in a vertical position for 30 s after the injection. SP was administered via the intraperitoneal route starting on the day of TNBS administration and continued daily until the end of the study at day 7. The mice were randomly divided into four groups: a control group given vehicle (CON), a colitis group given TNBS (TNBS), and two additional colitis groups receiving 5 nmol/kg or 10 nmol/kg of SP by injection (TNBS + SP-L and TNBS + SP-H, respectively). Each group consisted of six mice. Mice in the non-colitis group were treated with 0.1 ml of 50% ethanol alone instead of TNBS. Mice were weighed and observed daily, and assessed for DAI, based on the above-described criteria.

Statistical analysis

Data was analyzed, and graphs were plotted in the figures using GraphPad Prism software (Version 8.0, GraphPad, San Diego, CA, USA). Data are presented as the mean ± standard deviation (SD). Spearman's correlations among the phenotypes, colonic bacteria, metabolites, and brain gene expression were conducted utilizing the R software. Significant differences in more than two groups were analyzed using one-way analysis of variance (ANOVA) followed by Tukey's multiple comparisons test or two-way ANOVA with Sidak's multiple comparisons test. For all statistical comparisons, $^{*}p < 0.05$, $^{**}p < 0.01$, and $^{***}p < 0.001$.

Reporting summary

Further information on research design is available in the Nature Portfolio Reporting Summary linked to this article.

Data availability

16S rRNA sequence data have been deposited in the Sequence Read Archive (SRA) under BioProject accession numbers PRJNA1164042, PRJNA1277767 and PRJNA1279049. RNA-seq data have been deposited in the Gene Expression Omnibus (GEO) under accession number GSE278270. Metabolomics data have been deposited in the EMBL-EBI MetaboLights database under accession number MTBLS11203. All other data supporting the conclusions of this study are available in the paper and supplemental materials. Source data are provided with this paper.

References

1. Caruso, R., Lo, B. C. & Núñez, G. Host–microbiota interactions in inflammatory bowel disease. *Nat. Rev. Immunol.* **20**, 411–426 (2020).
2. Lee, K.-I. et al. Alleviating depressive-like behavior in DSS-induced colitis mice: Exploring naringin and poncirin from Poncirus trifoliata extracts. *Biomed. Pharmacother.* **175**, 116770 (2024).
3. Keefer, L. What can we do to tackle anxiety and depression in patients with inflammatory bowel disease? *Lancet Gastroenterol. Hepatol.* **6**, 337–338 (2021).
4. Tomazoni, E. I. & Benvegnú, D. M. Symptoms of anxiety and depression, and quality of life of patients with Crohn's disease. *Arquivos Gastroenterol.* **55**, 148–153 (2018).
5. Chiu, L. S. & Anderton, R. S. The role of the microbiota–gut–brain axis in long-term neurodegenerative processes following traumatic brain injury. *Eur. J. Neurosci.* **57**, 400–418 (2023).
6. Caso, J. R., Balanza-Martinez, V., Palomo, T. & Garcia-Bueno, B. The microbiota and gut-brain axis: contributions to the immunopathogenesis of schizophrenia. *Curr. Pharm. Des.* **22**, 6122–6133 (2016).
7. Qi, Y. et al. Walnut-derived peptide improves cognitive impairment in colitis mice induced by dextran sodium sulfate via the microbiota–gut–brain axis (MGBA). *J. Agric. Food Chem.* **71**, 19501–19515 (2023).
8. Kurokawa, S. et al. The effect of fecal microbiota transplantation on psychiatric symptoms among patients with irritable bowel syndrome, functional diarrhea and functional constipation: an open-label observational study. *J. Affect. Disord.* **235**, 506–512 (2018).
9. Banfi, D. et al. Impact of microbial metabolites on microbiota–gut–brain axis in inflammatory bowel disease. *Int. J. Mol. Sci.* **22**, 1623 (2021).
10. Leng, L. et al. Menin deficiency leads to depressive-like behaviors in mice by modulating astrocyte-mediated neuroinflammation. *Neuron* **100**, 551–563. e557 (2018).
11. Mass, M., Kubera, M. & Leunis, J.-C. The gut-brain barrier in major depression: intestinal mucosal dysfunction with an increased translocation of LPS from gram-negative enterobacteria (leaky gut) plays a role in the inflammatory pathophysiology of depression. *Neuroendocrinol. Lett.* **29**, 117–124 (2008).
12. Miller, A. H., Haroon, E., Raison, C. L. & Felger, J. C. Cytokine targets in the brain: impact on neurotransmitters and neurocircuits. *Depress. Anxiety* **30**, 297–306 (2013).
13. Roshan-Milani, S., Seyyedabadi, B., Saboory, E., Parsamanesh, N. & Mehranfard, N. Prenatal stress and increased susceptibility to anxiety-like behaviors: role of neuroinflammation and balance between GABAergic and glutamatergic transmission. *Stress* **24**, 481–495 (2021).

14. Kraft, A. D. & Harry, G. J. Features of microglia and neuroinflammation relevant to environmental exposure and neurotoxicity. *Int. J. Environ. Res. Public Health* **8**, 2980–3018 (2011).
15. Chen, L.-W., Yung, K.-L. & Chan, Y.-S. Reactive astrocytes as potential manipulation targets in novel cell replacement therapy of Parkinson's disease. *Curr. Drug Targets* **6**, 821–833 (2005).
16. Sofroniew, M. V. Multiple roles for astrocytes as effectors of cytokines and inflammatory mediators. *Neuroscientist* **20**, 160–172 (2014).
17. Cui, C., Grandison, L. & Noronha, A. *Neural-immune Interactions in Brain Function and Alcohol Related Disorders* (Springer Science & Business Media, 2012).
18. Giaume, C. & Venance, L. Intercellular calcium signaling and gap junctional communication in astrocytes. *Glia* **24**, 50–64 (1998).
19. Kirchhoff, F., Dringen, R. & Giaume, C. Pathways of neuron-astrocyte interactions and their possible role in neuroprotection. *Eur. Arch. Psychiatry Clin. Neurosci.* **251**, 159–169 (2001).
20. Collins, S. M., Surette, M. & Bercik, P. The interplay between the intestinal microbiota and the brain. *Nat. Rev. Microbiol.* **10**, 735–742 (2012).
21. Holzer, P. & Farzi, A. Neuropeptides and the microbiota-gut-brain axis. *Adv. Exp. Med. Biol.* **817**, 195–219 (2014).
22. Schwarz, M. J. & Ackenheil, M. The role of substance P in depression: therapeutic implications. *Dialog. Clin. Neurosci.* **4**, 21–29 (2002).
23. Hasenöhrl, R. et al. Substance P and its role in neural mechanisms governing learning, anxiety and functional recovery. *Neuropeptides* **34**, 272–280 (2000).
24. Kowall, N. W., Beal, M. F., Busciglio, J., Duffy, L. K. & Yankner, B. A. An in vivo model for the neurodegenerative effects of beta amyloid and protection by substance P. *Proc. Natl. Acad. Sci.* **88**, 7247–7251 (1991).
25. Nikolaus, S., Huston, J., Körber, B., Thiel, C. & Schwarting, R. Pretreatment with neurokinin substance P but not with cholecystokinin-8S can alleviate functional deficits of partial nigrostriatal 6-hydroxydopamine lesion. *Peptides* **18**, 1161–1168 (1997).
26. Lan, J. et al. Neuropeptide substance P attenuates colitis by suppressing inflammation and ferroptosis via the cGAS-STING signaling pathway. *Int. J. Biol. Sci.* **20**, 2507 (2024).
27. Randhawa, P. K., Singh, K., Singh, N. & Jaggi, A. S. A review on chemical-induced inflammatory bowel disease models in rodents. *Korean J. Physiol. Pharmacol.* **18**, 279 (2014).
28. Tang, X. Anti-inflammatory and intestinal microbiota modulation properties of Jinxiang garlic (Allium sativum L.) polysaccharides toward dextran sodium sulfate-induced colitis.pdf. (2021).
29. Niu, S. et al. Jatrorrhizine alleviates DSS-induced ulcerative colitis by regulating the intestinal barrier function and inhibiting TLR4/MyD88/NF-κB signaling pathway. *Evidence-Based Complement. Altern. Med.* **2022**, 3498310 (2022).
30. Nyström, E. E. et al. An intercrypt subpopulation of goblet cells is essential for colonic mucus barrier function. *Science* **372**, eabb1590 (2021).
31. Di Tommaso, N., Gasbarrini, A. & Ponziani, F. R. Intestinal barrier in human health and disease. *Int. J. Environ. Res. Public Health* **18**, 12836 (2021).
32. Thoo, L., Noti, M. & Krebs, P. Keep calm: the intestinal barrier at the interface of peace and war. *Cell Death Dis.* **10**, 849 (2019).
33. Shepherd, J. K., Grewal, S. S., Fletcher, A., Bill, D. J. & Dourish, C. T. Behavioural and pharmacological characterisation of the elevated "zero-maze" as an animal model of anxiety. *Psychopharmacology* **116**, 56–64 (1994).
34. Tartt, A. N., Mariani, M. B., Hen, R., Mann, J. J. & Boldrini, M. Dysregulation of adult hippocampal neuroplasticity in major depression: pathogenesis and therapeutic implications. *Mol. Psychiatry* **27**, 2689–2699 (2022).
35. Godsil, B. P., Kiss, J. P., Spedding, M. & Jay, T. M. The hippocampal–prefrontal pathway: the weak link in psychiatric disorders? *Eur. Neuropsychopharmacol.* **23**, 1165–1181 (2013).
36. Luo, L. et al. Scopoletin ameliorates anxiety-like behaviors in complete Freund's adjuvant-induced mouse model. *Mol. Brain* **13**, 1–13 (2020).
37. Regen, F., Hellmann-Regen, J., Costantini, E. & Reale, M. Neuroinflammation and Alzheimer's disease: implications for microglial activation. *Curr. Alzheimer Res.* **14**, 1140–1148 (2017).
38. Lee, H.-G., Wheeler, M. A. & Quintana, F. J. Function and therapeutic value of astrocytes in neurological diseases. *Nat. Rev. Drug Discov.* **21**, 339–358 (2022).
39. Chai, M. et al. Molecular mechanism of the protective effects of M2 microglia on neurons: a review focused on exosomes and secretory proteins. *Neurochem. Res.* **47**, 3556–3564 (2022).
40. Wlodarska, M. et al. Antibiotic treatment alters the colonic mucus layer and predisposes the host to exacerbated citrobacter rodentium-induced colitis. *Infect. Immun.* **79**, 1536–1545 (2011).
41. Choudhary, S. et al. Novel antioxidants zolimid and AEOL11201 ameliorate colitis in rats. *Digest. Dis. Sci.* **46**, 2222 (2001).
42. Negri, S. et al. GABAA and GABAB receptors mediate GABA-induced intracellular Ca2+ signals in human brain microvascular endothelial cells. *Cells* **11**, 3860 (2022).
43. Ruey-Horng, S., Chen-Yu, W. & Chuen-Mao, Y. NF-kappaB signaling pathways in neurological inflammation: a mini review. *Front. Mol. Neurosci.* **8**, 77 (2015).
44. Sidoryk-Wegrzynowicz, M., Wegrzynowicz, M., Lee, E., Bowman, A. B. & Aschner, M. Role of astrocytes in brain function and disease. *Toxicol. Pathol.* **39**, 115 (2011).
45. Ahmed, H. et al. Microbiota-derived metabolites as drivers of gut–brain communication. *Gut microbes* **14**, 2102878 (2022).
46. Grill. et al. Intestinal E-cadherin deficiency aggravates dextran sodium sulfate-induced colitis.
47. Yogeswara, I. B. A., Maneerat, S. & Haltrich, D. Glutamate decarboxylase from lactic acid bacteria—a key enzyme in GABA synthesis. *Microorganisms* **8**, 1923 (2020).
48. Lee, T.-S. et al. GAT1 and GAT3 expression are differently localized in the human epileptogenic hippocampus. *Acta Neuropathol.* **111**, 351–363 (2006).
49. Neurath, M. F., Fuss, I., Kelsall, B. L., Stüber, E. & Strober, W. Antibodies to interleukin 12 abrogate established experimental colitis in mice. *J. Exp. Med.* **182**, 1281–1290 (1995).
50. Liu, J. et al. Protective effects and mechanisms of HuDiChangRong capsule on TNBS-induced ulcerative colitis in mice. *J. Ethnopharmacol.* **337**, 118879 (2025).
51. Hong, C.-J., Chen, S.-Y., Hsu, Y.-H. & Yen, G.-C. Protective effect of fermented okara on the regulation of inflammation, the gut microbiota, and SCFAs production in rats with TNBS-induced colitis. *Food Res. Int.* **157**, 111390 (2022).
52. O'Connor, T. M. et al. The role of substance P in inflammatory disease. *J. Cell. Physiol.* **201**, 167–180 (2004).
53. Hurst, S. M., Stanisz, A. M., Sharkey, K. A. & Collins, S. M. Interleukin 1 beta-induced increase in substance P in rat myenteric plexus. *Gastroenterology* **105**, 1754–1760 (1993).
54. Engel, M. A. et al. TRPA1 and substance P mediate colitis in mice. *Gastroenterology* **141**, 1346–1358 (2011).
55. Weinstock, J. V. et al. Substance P regulates Th1-type colitis in IL-10 knockout mice. *J. Immunol.* **171**, 3762–3767 (2003).
56. Qin, Y. Y. et al. Neuropeptide Y attenuates cardiac remodeling and deterioration of function following myocardial infarction. *Mol. Ther.: J. Am. Soc. Gene Ther.* **30**, 881–897 (2022).
57. Koon, H. W., Zhao, D., Zhan, Y., Moyer, M. P. & Pothoulakis, C. Substance P mediates antiapoptotic responses in human colonocytes by Akt activation. *Proc. Natl. Acad. Sci. USA* **104**, 2013–2018 (2007).

58. Leal, E. C. et al. Substance P promotes wound healing in diabetes by modulating inflammation and macrophage phenotype. *Am. J. Pathol.* **185**, 1638–1648 (2015).
59. Hong, H. S. et al. Substance-P alleviates dextran sulfate sodium-induced intestinal damage by suppressing inflammation through enrichment of M2 macrophages and regulatory T cells. *Cytokine* **90**, 21–30 (2017).
60. Kim, D. Y., Piao, J. & Hong, H. S. Substance-P inhibits cardiac microvascular endothelial dysfunction caused by high glucose-induced oxidative stress. *Antioxidants* **10**, 1084 (2021).
61. Kim, S. & Hong, H. S. Substance-P prevents the cholestatic liver injury by regulating inflammatory responses. *Peptides* **137**, 170494 (2021).
62. Delgado, A. V., McManus, A. T. & Chambers, J. P. Exogenous administration of substance P enhances wound healing in a novel skin-injury model. *Exp. Biol. Med.* **230**, 271–280 (2005).
63. Kumar, S., Tan, Y. & Berthiaume, F. Neuropeptide substance P enhances skin wound healing in vitro and in vivo under hypoxia. *Biomedicines* **9**, 222 (2021).
64. Boonstra, E. et al. Neurotransmitters as food supplements: the effects of GABA on brain and behavior. *Front. Psychol.* **6**, 167121 (2015).
65. Szőke, H. et al. Gut dysbiosis and serotonin: intestinal 5-HT as a ubiquitous membrane permeability regulator in host tissues, organs, and the brain. *Rev. Neurosci.* **31**, 415–425 (2020).
66. Xia, Y. et al. GABA attenuates ETEC-induced intestinal epithelial cell apoptosis involving GABA AR signaling and the AMPK-autophagy pathway. *Food Funct.* **10**, 7509–7522 (2019).
67. Ahn, W., Chi, G., Kim, S., Son, Y. & Zhang, M. Substance P reduces infarct size and mortality after ischemic stroke, possibly through the M2 polarization of microglia/macrophages and neuroprotection in the ischemic rat brain. *Cell. Mol. Neurobiol.* **43**, 2035–2052 (2023).
68. Khairova, R. A., Machado-Vieira, R., Du, J. & Manji, H. K. A potential role for pro-inflammatory cytokines in regulating synaptic plasticity in major depressive disorder. *Int. J. Neuropsychopharmacol.* **12**, 561–578 (2009).
69. Setiawan, E. et al. Role of translocator protein density, a marker of neuroinflammation, in the brain during major depressive episodes. *JAMA Psychiatry* **72**, 268–275 (2015).
70. Zhao, B. et al. Lycopene alleviates DSS-induced colitis and behavioral disorders via mediating microbes-gut–brain axis balance. *J. Agric. Food Chem.* **68**, 3963–3975 (2020).
71. Zhang, J. et al. Curcumin inhibits LPS-induced neuroinflammation by promoting microglial M2 polarization via TREM2/TLR4/NF-κB pathways in BV2 cells. *Mol. Immunol.* **116**, 29–37 (2019).
72. Colombo, E. & Farina, C. Astrocytes: key regulators of neuroinflammation. *Trends Immunol.* **37**, 608–620 (2016).
73. Cho, W.-H. et al. Hippocampal astrocytes modulate anxiety-like behavior. *Nat. Commun.* **13**, 6536 (2022).
74. Cobb, J. A. et al. Density of GFAP-immunoreactive astrocytes is decreased in left hippocampi in major depressive disorder. *Neuroscience* **316**, 209–220 (2016).
75. Dewalt, G. J. et al. Region-specific alterations in astrocyte and microglia morphology following exposure to blasts in the mouse hippocampus. *Neurosci. Lett.* **664**, 160–166 (2018).
76. Zhang, N., Zhang, Q., Xie, L., Li, C. & Yu, S. Electroacupuncture and moxibustion regulate hippocampus glia and mitochondria activation in DSS-induced colitis mice. *Evid.-based Complement. Altern. Med.* **2020**, 1–11 (2020).
77. Zhao, X., Ahram, A., Berman, R. F., Muizelaar, J. P. & Lyeth, B. G. Early loss of astrocytes after experimental traumatic brain injury. *Glia* **44**, 140–152 (2010).
78. Dickerson, M. R., Murphy, S. F., Urban, M. J., White, Z. & VandeVord, P. J. Chronic anxiety-and depression-like behaviors are associated with glial-driven pathology following repeated blast induced neurotrauma. *Front. Behav. Neurosci.* **15**, 787475 (2021).
79. Do, J. & Woo, J. From gut to brain: alteration in inflammation markers in the brain of dextran sodium sulfate-induced colitis model mice. *Clin. Psychopharmacol. Neurosci.* **16**, 422 (2018).
80. Zhang, Y. et al. Gut microbiota from NLRP3-deficient mice ameliorates depressive-like behaviors by regulating astrocyte dysfunction via circHIPK2. *Microbiome* **7**, 1–16 (2019).
81. Cryan, J. F. et al. The microbiota-gut-brain axis. *Physiol. Rev.* **99**, 1877–2013 (2019).
82. De Santa, F. et al. Effect of a multi-strain probiotic mixture consumption on anxiety and depression symptoms induced in adult mice by postnatal maternal separation. *Microbiome* **12**, 29 (2024).
83. Ma, J., Wang, R., Chen, Y., Wang, Z. & Dong, Y. 5-HT attenuates chronic stress-induced cognitive impairment in mice through intestinal flora disruption. *J. Neuroinflammation* **20**, 23 (2023).
84. Zhao, Y. et al. Effects of GABA supplementation on intestinal SIgA secretion and gut microbiota in the healthy and ETEC-infected weanling piglets. *Mediat. Inflamm.* **2020**, 7368483 (2020).
85. Biaggini, K. et al. Substance P enhances lactic acid and tyramine production in Enterococcus faecalis V583 and promotes its cytotoxic effect on intestinal Caco-2/TC7 cells. *Gut Pathog.* **9**, 1–8 (2017).
86. Ye, Z.-W. et al. Fucoidan attenuates chronic colitis and behavioral deficits by reshaping gut microbiota-brain axis balance. *J. Funct. Foods* **112**, 105951 (2024).
87. Shin, N.-R., Whon, T. W. & Bae, J.-W. Proteobacteria: microbial signature of dysbiosis in gut microbiota. *Trends Biotechnol.* **33**, 496–503 (2015).
88. Pei, L. -y et al. Regulatory effect of Garidisan on dysbiosis of the gut microbiota in the mouse model of ulcerative colitis induced by dextran sulfate sodium. *BMC Complement. Altern. Med.* **19**, 1–11 (2019).
89. Zhu, Y. et al. Exploration of the muribaculaceae family in the gut microbiota: diversity, metabolism, and function. *Nutrients* **16**, 2660 (2024).
90. Qian, J. et al. Periodontitis salivary microbiota exacerbates colitis-induced anxiety-like behavior via gut microbiota. *npj Biofilms Microbiomes* **9**, 93 (2023).
91. Jang, H.-M. et al. Enterococcus faecium and Pediococcus acidilactici deteriorate Enterobacteriaceae-induced depression and colitis in mice. *Sci. Rep.* **12**, 9389 (2022).
92. Marotta, A. et al. Effects of probiotics on cognitive reactivity, mood, and sleep quality. *Front. Psychiatry* **10**, 164 (2019).
93. Jang, H. M. et al. Transplantation of fecal microbiota from patients with inflammatory bowel disease and depression alters immune response and behavior in recipient mice. *Sci. Rep.* **11**, 20406 (2021).
94. Chinna Meyyappan, A., Forth, E., Wallace, C. J. K. & Milev, R. Effect of fecal microbiota transplant on symptoms of psychiatric disorders: a systematic review. *BMC Psychiatry* **20**, 299 (2020).
95. Xu, J. et al. Urolithins attenuate LPS-induced neuroinflammation in BV2Microglia via MAPK, Akt, and NF-κB signaling pathways. *J. Agric. Food Chem.* **66**, 571–580 (2018).
96. Maguire, J. & Mody, I. GABAAR plasticity during pregnancy: relevance to postpartum depression. *Neuron* **59**, 207–213 (2008).
97. Möhler, H. The GABA system in anxiety and depression and its therapeutic potential. *Neuropharmacology* **62**, 42–53 (2012).
98. Kumar, K., Sharma, S., Kumar, P. & Deshmukh, R. Therapeutic potential of GABAB receptor ligands in drug addiction, anxiety, depression and other CNS disorders. *Pharmacol. Biochem. Behav.* **110**, 174–184 (2013).
99. Barker, J. et al. GABAergic cells and signals in CNS development. *Perspect. Dev. Neurobiol.* **5**, 305–322 (1998).

100. Ben-Ari, Y., Gaiarsa, J.-L., Tyzio, R. & Khazipov, R. GABA: a pioneer transmitter that excites immature neurons and generates primitive oscillations. *Physiol. Rev.* **87**, 1215–1284 (2007).
101. Owens, D. F. & Kriegstein, A. R. Is there more to GABA than synaptic inhibition? *Nat. Rev. Neurosci.* **3**, 715–727 (2002).
102. Hirono, M., Yoshioka, T. & Konishi, S. GABAB receptor activation enhances mGluR-mediated responses at cerebellar excitatory synapses. *Nat. Neurosci.* **4**, 1207–1216 (2001).
103. Tabata, T. et al. Ca2+ activity at GABAB receptors constitutively promotes metabotropic glutamate signaling in the absence of GABA. *Proc. Natl. Acad. Sci.* **101**, 16952–16957 (2004).
104. Schwirtlich, M. et al. GABAA and GABAB receptors of distinct properties affect oppositely the proliferation of mouse embryonic stem cells through synergistic elevation of intracellular Ca2+. *FASEB J.* **24**, 1218–1228 (2010).
105. Sałaciak, K., Koszałka, A., Żmudzka, E. & Pytka, K. The calcium/calmodulin-dependent kinases II and IV as therapeutic targets in neurodegenerative and neuropsychiatric disorders. *Int. J. Mol. Sci.* **22**, 4307 (2021).
106. Zhang, M. et al. Structural basis for calmodulin as a dynamic calcium sensor. *Structure* **20**, 911–923 (2012).
107. Czéh, B., Simon, M., Schmelting, B., Hiemke, C. & Fuchs, E. Astroglial plasticity in the hippocampus is affected by chronic psychosocial stress and concomitant fluoxetine treatment. *Neuropsychopharmacology* **31**, 1616–1626 (2006).
108. Salvo-Romero, E., Stokes, P. & Gareau, M. G. Microbiota-immune interactions: from gut to brain. *LymphoSign J.* **7**, 1–23 (2020).
109. Strandwitz, P. Neurotransmitter modulation by the gut microbiota. *Brain Res.* **1693**, 128–133 (2018).
110. He, Y. et al. Intervention mechanism of repeated oral GABA administration on anxiety-like behaviors induced by emotional stress in rats. *Psychiatry Res.* **271**, 649–657 (2019).
111. Zarrindast, M.-R. & Khakpai, F. The modulatory role of dopamine in anxiety-like behavior. *Arch. Iran. Med.* **18**, 0–0 (2015).
112. Wu, S. -e. et al. Microbiota-derived metabolite promotes HDAC3 activity in the gut. *Nature* **586**, 108–112 (2020).
113. Shirmohammad, F., Mehri, M. & Joezy-Shekalgorabi, S. A review on the role of inositol in aquaculture. (2016).
114. Su, X. B., Ko, A.-L. A. & Saiardi, A. Regulations of myo-inositol homeostasis: mechanisms, implications, and perspectives. *Adv. Biol. Regul.* **87**, 100921 (2023).
115. Vaz, S. H. et al. Brain-derived neurotrophic factor (BDNF) enhances GABA transport by modulating the trafficking of GABA transporter-1 (GAT-1) from the plasma membrane of rat cortical astrocytes. *J. Biol. Chem.* **286**, 40464–40476 (2011).
116. Zhou, F. et al. Electroacupuncture attenuated anxiety and depression-like behavior via inhibition of hippocampal inflammatory response and metabolic disorders in TNBS-induced IBD rats. *Oxid. Med. Cell. Longev.* **2022**, 8295580 (2022).
117. Wu, Y. et al. Deferasirox alleviates DSS-induced ulcerative colitis in mice by inhibiting ferroptosis and improving intestinal microbiota. *Life Sci.* **314**, 121312 (2023).
118. Dong, S. et al. Dihydromyricetin improves DSS-induced colitis in mice via modulation of fecal-bacteria-related bile acid metabolism. *Pharmacol. Res.* **171**, 105767 (2021).
119. Wang, Y. et al. Modified gegen qinlian decoction regulates Treg/Th17 balance to ameliorate DSS-induced acute experimental colitis in mice by altering the gut microbiota. *Front. Pharmacol.* **12**, 756978 (2021).
120. Chen, X. et al. Moderate dietary protein restriction optimized gut microbiota and mucosal barrier in growing pig model. *Front. Cell. Infect. Microbiol.* **8**, 246 (2018).
121. Ma, N. et al. Poly-β-hydroxybutyrate alleviated diarrhea and colitis via Lactobacillus johnsonii biofilm-mediated maturation of sulfomucin. *Sci. China Life Sci.* **66**, 1569–1588 (2023).
122. Song, A.-Q. et al. NLRP1 inflammasome contributes to chronic stress-induced depressive-like behaviors in mice. *J. Neuroinflammation* **17**, 1–13 (2020).
123. Callahan, B. J. et al. DADA2: High-resolution sample inference from Illumina amplicon data. *Nat. Methods* **13**, 581–583 (2016).
124. Bolyen, E. et al. Reproducible, interactive, scalable and extensible microbiome data science using QIIME 2. *Nat. Biotechnol.* **37**, 852–857 (2019).
125. Douglas, G. M. et al. PICRUSt2 for prediction of metagenome functions. *Nat. Biotechnol.* **38**, 685–688 (2020).
126. Ogata, H. et al. KEGG: Kyoto Encyclopedia of Genes and Genomes. *Nucleic Acids Res.* **27**, 29–34 (1999).
127. Love, M. I., Huber, W. & Anders, S. Moderated estimation of fold change and dispersion for RNA-seq data with DESeq2. *Genome Biol.* **15**, 1–21 (2014).
128. Chandrashekar, D. S. et al. UALCAN: a portal for facilitating tumor subgroup gene expression and survival analyses. *Neoplasia* **19**, 649–658 (2017).
129. Smith, C. A. et al. METLIN: a metabolite mass spectral database. *Ther. Drug Monit.* **27**, 747–751 (2005).
130. Chong, J. & Xia, J. MetaboAnalystR: an R package for flexible and reproducible analysis of metabolomics data. *Bioinformatics* **34**, 4313–4314 (2018).
131. Chen, G. et al. Sodium butyrate inhibits inflammation and maintains epithelium barrier integrity in a TNBS-induced inflammatory bowel disease mice model. *EBioMedicine* **30**, 317–325 (2018).

Acknowledgements

This work was supported by the Beijing Municipal Natural Science Foundation (6232021 to Y.M.), National Natural Science Foundation of China (31772686 to Y.M.), National Key Research and Development Program of China (2022YFD1801105 to Z.H.), and the 2115 Talent Development Program of China Agricultural University (00109015 to Z.H. and Y.M.).

Author contributions

Y.M. and J.L. conceived and designed the study. J.L. collected all the data from the experiment. J.L., J.W., S.H., C.L. and Z.D. conducted statistical analyses. J.L. wrote the paper. Y.M., J.L. and Z.H. revised the manuscript. Z.D. provided technical support. Z.H. provided technical and material support. Y.M. supervised the study and provided administrative, technical and material support. All the authors approved the final version of the manuscript.

Competing interests

The authors declare no competing interests.

Additional information

Supplementary information The online version contains supplementary material available at https://doi.org/10.1038/s41467-025-67904-0.

Correspondence and requests for materials should be addressed to Yunfei Ma.

Peer review information *Nature Communications* thanks Stephen Collins and the other, anonymous, reviewer(s) for their contribution to the peer review of this work. A peer review file is available.